International Communications in Heat and Mass Transfer 171 (2026) 110097

Contents lists available at ScienceDirect

International Communications in Heat and Mass Transfer

journal homepage: www.elsevier.com/locate/ichmt

Large eddy simulation in optimization of fan-shaped cooling holes using modal subdivision design variables

Ali Zamiri [a],*, Sam Lovett [a], Daniel J. Poole [a], Thomas C.S. Rendall [a], C.B. Allen [a], Giovanna Barigozzi [b], Jin Taek Chung [c]

[a] Department of Aerospace Engineering, University of Bristol, United Kingdom
[b] Department of Engineering and Applied Sciences, University of Bergamo, Dalmine, Italy
[c] School of Mechanical Engineering, Korea University, Seoul, Republic of Korea

ARTICLE INFO

Keywords:
Gas turbine
Film cooling technique
Laidback fan-shaped cooling hole
Modal shape parameterization

ABSTRACT

In advanced gas turbine engines, fan-shaped cooling holes are widely employed to protect turbine components from the high-temperature mainstream flow. The geometric characteristics of these holes are critical in determining the film-cooling effectiveness. Therefore, identifying an optimal hole configuration is essential to enhance thermal protection and overall cooling performance. In this study, a large eddy simulation (LES) approach was conducted to investigate the influences of surface geometry modifications on the film-cooling effectiveness and turbulent flow structures for a 7-7-7 laidback fan-shaped cooling hole (7-degree expansion angle in each direction). The cooling hole was located on a flat plate with a 30-degree injection angle, operating at a constant density and blowing ratio of 1.5. A novel modal shape parameterization technique was introduced to systematically modify the hole surface geometry, providing a compact physic-based representation of complex shape variations. Eight designed cases were generated using Latin Hypercube sampling (LHS) based on two shape parameters: mode number and mode amplitude. The area-averaged film-cooling effectiveness on the flat plate was selected as the objective function. A genetic aggregation method was adopted to construct a response surface model using the LES data. Subsequently, a multi-objective genetic algorithm (MOGA) was used to identify the optimal surface geometry. The results indicated a substantial improvement in cooling effectiveness across all modified configurations compared to the reference case. The optimized design demonstrated reduced internal turbulent fluctuations within the cooling hole and diminished flow disturbances in the interaction region with the mainstream, resulting in a 22% improvement in cooling performance—from 0.2028 to 0.2475—compared to the reference configuration.

1. Introduction

Components of modern gas turbine systems operate at extremely high temperatures to achieve greater thermal efficiency. To enhance thermal performance, turbine inlet temperature has been increased to approximately 2000 K [1,2], significantly exceeding the melting point of turbine blade materials. As a result, effective active techniques are essential to protect the turbine blades from the hot mainstream combusted gases and to extend the lifespan of turbine components.

One of the thermal protection techniques widely applied in advanced gas turbine engines is the film-cooling technique. In this method, relatively cooler air from the compressor section is injected through discrete small holes on the blade surfaces, forming a thin, cooler layer on the surfaces that prevents direct contact between the hot mainstream flow and the turbine blades [3–5]. Although film cooling enhances turbine efficiency by enabling higher turbine inlet temperatures, it also reduces aerodynamic performance due to the interaction between the coolant jet and the mainstream flows, referred to the coolant jet cross-flow, which increases mixing losses. Therefore, improving cooling effectiveness while minimizing coolant usage is essential to reduce flow disturbances in the interaction region.

Numerous studies have demonstrated that both operational and geometrical factors significantly influence the effectiveness of film cooling techniques [6–9]. Key geometrical parameters of cooling holes include hole shape, length-to-diameter ratio, expansion and injection angles. Various types of cooling holes have been developed, including conventional cylindrical holes [10], shaped holes [11,12], diffusion slot holes [13], cat-ear hole [14], and double jet holes [15]. Many investigations have examined how the geometrical features of cylindrical holes

* Corresponding author.
E-mail address: ali.en.zamiri@gmail.com (A. Zamiri).

https://doi.org/10.1016/j.icheatmasstransfer.2025.110097

Available online 20 November 2025

Nomenclature

A	Mode amplitude
C_w	WALE constant
D	Cooling hole diameter
DOE	Cooling hole diameter
DR	Density ratio
e	Total energy
H	Energy flux generated by thermal energy and work done by total stress
L	Cooling hole length
LHS	Latin Hypercube sampling
M	Blowing ratio
N	Mode number
P	Pitch distance
p	Pressure
SGS	Subgrid scale
T	Temperature
u	Velocity
WALE	Wall-adapting local eddy viscosity

Greek symbols

α	Injection angle
β	Forward expansion angle
γ	Lateral expansion angle
ρ	Density
η	Film-cooling effectiveness
$\bar{\eta}$	Lateral averaged film-cooling effectiveness
$\bar{\bar{\eta}}$	Area averaged film-cooling effectiveness
θ	Non-dimensional temperature
μ	Eddy viscosity
σ	Molecular viscous stress tensor
τ	Stress tensor

Sub-, Superscripts

fwd	Forward
j	Jet
m	Metering

affect cooling performance [10,16,17]. Over the past five decades, shaped holes have consistently shown superior film cooling effectiveness compared to cylindrical ones, primarily due to more uniform lateral coolant distribution and reduced jet lift-off, particularly at high blowing ratios [7,11,18]. Goldstein et al. [7] showed that the use of a cooling hole with an initially cylindrical shape widened to each side by a 10-degree angle significantly enhances film cooling performance immediately downstream of the hole exit at various density ratios. Bunker [18] provided a comprehensive review of shaped cooling hole configurations applied in turbine film cooling technology, concluding that these designs result in lower-momentum coolant injection jets with broader surface coverage and continuously increasing effectiveness with blowing ratio. Zamiri et al. [19] conducted numerical simulations to investigate the effects of different geometrical parameters of shaped cooling holes on film cooling effectiveness. Their results showed that reducing the metering length enhanced the overall cooling effectiveness on the flat plate surface. Moreover, it was found that increasing the lateral expansion angle improved both the lateral and area-averaged cooling effectiveness. Given the widespread adoption of fan-shaped cooling holes in the gas turbine industry for their enhanced cooling performance, further research is necessary to explore alternative geometries and identify optimal cooling hole configurations for improved thermal protection.

Several experimental studies have been conducted to optimize the film cooling effectiveness of shaped holes. Park et al. [20] experimentally investigated the influence of shape parameters of fan-shaped holes on cooling performance using the pressure sensitive paint (PSP) technique over a wide range of blowing and density ratios. Their results showed that the overall cooling performance increased with larger lateral and forward expansion angles, and the optimized cooling hole design improved cooling effectiveness by approximately 50% compared to the reference hole. Jo et al. [21] examined the impact of geometric variables on the film cooling performance of compound angled asymmetric laidback fan-shaped holes. In this study, the leeward and windward expansion angles were selected as design variables, and a Kriging optimization algorithm was employed to determine the optimal values. It was indicated that increasing the expansion angles significantly improved overall cooling effectiveness, with the optimized configuration offering a 1.3% improvement in cooling effectiveness over the reference cooling hole. Jeong et al. [22] performed an experimental-based optimization to determine the optimal shape of a butterfly-shaped cooling hole using the design of experiment (DOE) methodology. Three geometrical parameters, forward expansion angle, lateral expansion angle, and twist angle, were chosen as design variables under constant blowing and density ratios of 2. The optimal configuration demonstrated an approximate 8% improvement in cooling effectiveness relative to the baseline case. As the shape of the cooling hole significantly affects film cooling performance downstream of the hole exit, accurately predicting cooling effectiveness is essential. Although experimental techniques offer high measurement accuracy, advancement in numerical schemes and high-performance computational resources have led researchers to increasingly rely on computational fluid dynamics (CFD) approaches to predict the heat transfer characteristics due to their cost- and time-efficiency.

Most numerical studies on film cooling hole optimization have been conducted using the RANS (Reynolds averaged Navier–Stokes) approach [23–25]. Zhang et al. [24] developed an optimization framework for film cooling hole shape design using RANS simulations to achieve maximum cooling performance at an affordable computational cost. Their results showed that the spatially averaged cooling performance improved by 39% compared to the reference case. Jones et al. [25] employed a RANS-based CFD method to investigate a wide range of forward and lateral expansion angles for turbine film cooling holes. The optimal configuration was found to be a hole with a 15-degree lateral and a 1-degree forward expansion angle, resulting in a 40% improvement in cooling effectiveness. While the RANS approach can reasonably predict flow fields, it tends to overpredict thermal fields, particularly in complex flows like film cooling flows, due to turbulence closure models that simplify the physics of turbulence. Therefore, high-fidelity CFD approaches such as large eddy simulation (LES) are required to resolve near-wall turbulence structures accurately and capture the three-dimensional flow and thermal field characteristics within fan-shaped holes [26–30]. Agarwal et al. [27] performed a shaped hole optimization approach based on an LES method and efficient global optimization. They sampled forty design cases and the optimized hole showed significantly improved cooling effectiveness compared to the baseline 7-7-7 fan-shaped cooling hole. Zamiri et al. [31] conducted an LES-based optimization procedure to maximize area-averaged cooling performance, achieving a 50% improvement in cooling effectiveness over the reference cooling hole. Since fan-shaped cooling holes are widely implemented in advanced gas turbines, further studies are needed to identify optimal shape configurations for enhancing film cooling effectiveness. Although numerous experimental and numerical studies have reported on optimization of cooling hole geometry, most of these studies have focused on geometric parameters such as lateral expansion angle, forward expansion angle, metering

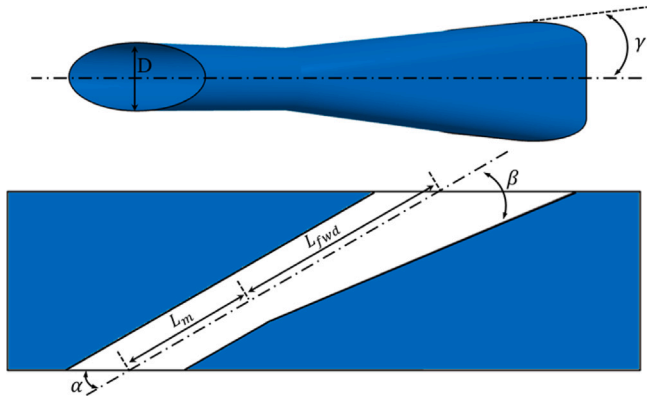

Fig. 1. Schematic view of baseline 7-7-7 laidback fan-shaped cooling hole.

length, and diameter-to-length ratio. To our knowledge, no publication has investigated surface shape optimization of fan-shaped cooling holes using a shape parameterization method in combination with LES simulations.

In the current numerical analysis, a combined LES approach and modal shape parameterization-based optimization strategy was applied, for the first time, to optimize the surface geometry of a laidback fan-shaped cooling hole to enhance cooling performance. A 3D, unsteady, compressible LES approach was carried out using Simcenter STAR-CCM+ V2302 for various fan-shaped cooling hole configurations located on a flat plate, under constant density and blowing ratio of 1.5. The LES results for the reference case were validated against experimental data [11] in terms of both flow and thermal fields. The main objective of this study is to evaluate the potential of the combined LES and modal shape parameterization approach in optimizing the film-cooling effectiveness (η) of a laidback fan-shaped hole. Two key design variables in the modal shape parameterization method, mode number (N) and mode amplitude (A), were chosen, and the area-averaged cooling effectiveness ($\bar{\eta}$) was used as the objective function. The Latin Hypercube sampling (LHS) method was utilized as the DOE approach to generate eight different cooling hole geometries. A genetic aggregation optimization algorithm was then employed to construct the response surface based on LES results and identify the optimal cooling hole configuration. The proposed LES/modal shape parameterization framework demonstrates strong potential as a robust tool for optimizing cooling hole surface geometry, offering significant value for advanced gas turbine cooling design.

2. Numerical method

2.1. Film cooling hole specifications

The film cooling hole investigated in this study is the 7-7-7 laidback fan-shaped cooling hole [11], as shown in Fig. 1. The cooling hole is located on a flat plate with a 30° injection angle (α) relative to the mainstream flow direction. The lateral (γ) and forward (β) expansion angles are 7°. The cooling hole has a diameter (D) of 7.75 mm and an overall length of $6D$, including a metering section of $2.5D$ and a diffuser section of $3.5D$. The holes are arranged with a lateral spacing of $6D$, which is intended to reduce interaction effects between adjacent coolant jets. Table 1 summarizes the detailed specifications of the 7-7-7 fan-shaped cooling hole. Film-cooling effectiveness was obtained from surface temperature measurements using a FLIR SC62 infrared camera [11]. Further geometric details of the cooling hole and a comprehensive description of the experimental setup can be found in [11].

Fig. 2 presents a schematic view of the baseline cooling hole and a modified cooling hole configuration developed using a modal shape

Table 1
Baseline cooling hole specification.

Cooling hole diameter (D)	7.75 mm
Injection angle (α)	30°
Overall length (L)	$6D$
Metering length (L_m)	$2.5D$
Forward length (L_{fwd})	$3.5D$
Forward expansion angle (β)	7°
Lateral expansion angle (γ)	7°
Pitch distance (P)	$6D$

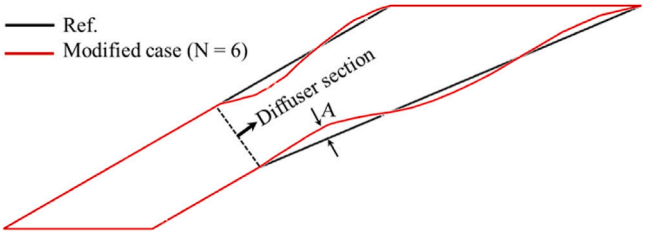

Fig. 2. Comparison of cooling hole surface profiles on the mid-span plane for the reference case and modified case based on modal shape parameterization technique.

parameterization technique on the mid-span plane. As shown, two different parameters, mode number (N) and mode amplitude (A), were considered as design variables to investigate the influence of cooling hole surface shape variations on film cooling performance. It should be noted that the modal deformation was applied exclusively to the diffuser section of the cooling hole, while the metering section remained unchanged throughout the study.

2.2. Numerical domain and grid

Figs. 3(a) and (b) present the computational domain and grid configuration for the modified cooling hole designed by the shape modal parameterization technique. The mainstream flow channel is defined as a 100D × 20D × 6D in the streamwise, normal, and spanwise directions, respectively. The coolant supply chamber is modeled as a 10D × 12D × 6D box. The mainstream inlet is positioned $35D$ upstream of the cooling hole exit to ensure the development of the inlet boundary layer. To promote the formation of a turbulent boundary layer, a tripping wire ($0.25D$) is located $15D$ downstream of the mainstream inlet. Fig. 3(b) shows a detailed view of the computational mesh on the mid-span cutting plane and within the diffuser section of the cooling hole. The numerical mesh, generated using Simcenter STAR-CCM+ V2302 software, consists of approximately 11,000,000 mesh elements. Polyhedral cells in combination with 21 prism layers near all solid surfaces were generated, which provide a balanced solution for complex mesh generation problems. As shown in the figure, local mesh refinement zones were applied within the cooling hole and near the flat plate surface to ensure sufficient grid resolution for the LES simulations. The maximum grid spacing in the streamwise (Δx^+), spanwise (Δz^+), and wall-normal (y^+) directions were 20, 10 and 0.25, respectively, which fall within the recommended range for LES simulations [32]. As shown in Fig. 3(b), the y^+ distribution on the cooling hole surfaces is maintained below 0.3. It should be noted that the current meshing strategy and grid resolution were selected based on the authors' previous studies [28–31].

2.3. Solver setup

The governing equations for the LES approach are obtained from the compressible, time-dependent, three-dimensional Navier–Stokes equations [32] by applying a spatial filtering operation. The filtered continuity, momentum, and energy equations are given in Eqs. (1)–(3),

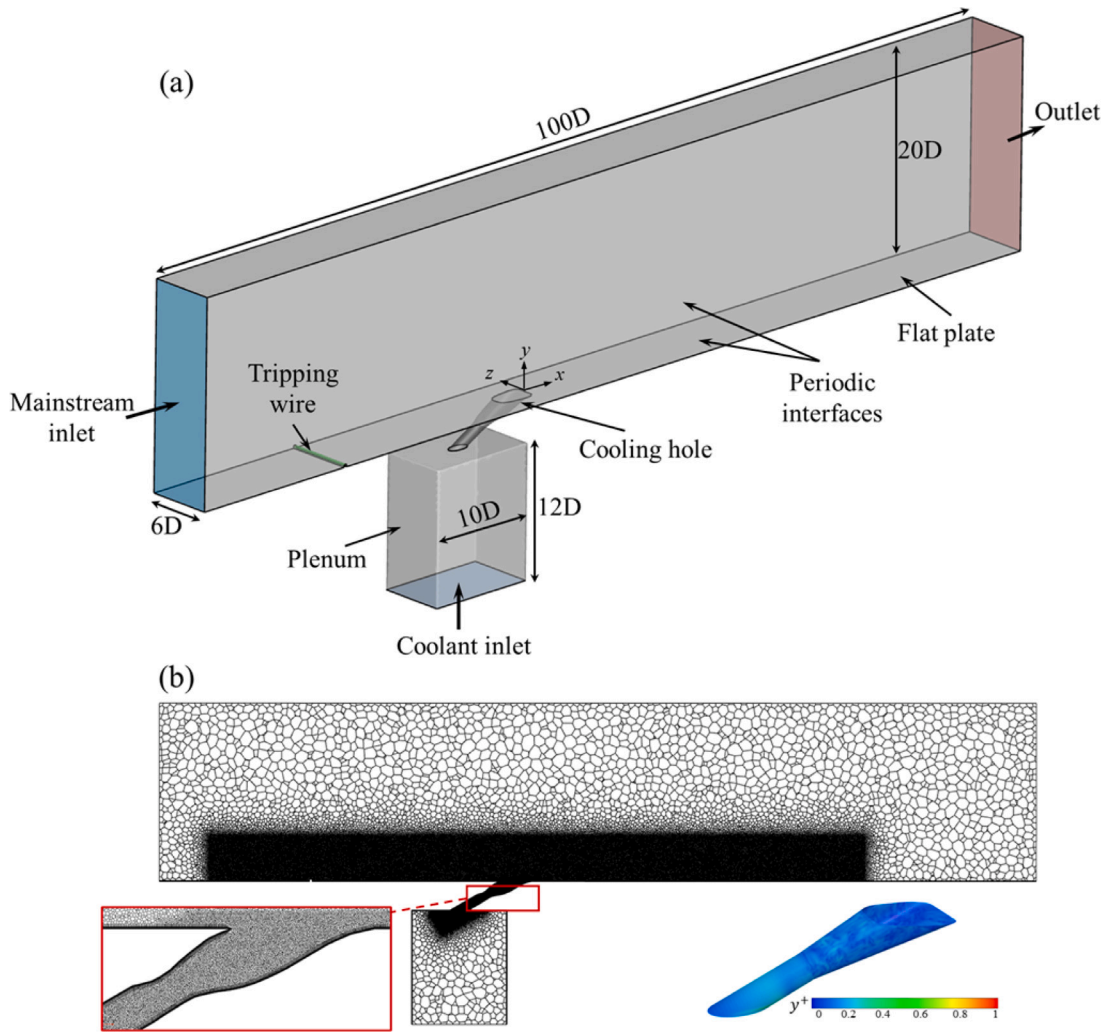

Fig. 3. Modified case based on modal shape parameterization technique: (a) computational domain, (b) computational grid on the mid-span cutting plane.

respectively.

$$\frac{\partial \rho}{\partial t} + \frac{\partial (\rho \tilde{u}_j)}{\partial x_j} = 0 \tag{1}$$

$$\frac{\partial (\rho \tilde{u}_i)}{\partial t} + \frac{\partial}{\partial x_j}(\rho \tilde{u}_i \tilde{u}_j) = -\frac{\partial p}{\partial x_i} + \frac{\partial \tau_{ij}^{LES}}{\partial x_j} + \frac{\partial \sigma_{ij}}{\partial x_j} \tag{2}$$

$$\frac{\partial (\rho \tilde{e})}{\partial t} + \frac{\partial}{\partial x_j}(\rho \tilde{e} + p)\,\tilde{u}_j = \frac{\partial H_j}{\partial x_j} \tag{3}$$

where ρ, $\tilde{u}$, p and $\tilde{e}$ are density, velocity, pressure and total energy, respectively. H is the flux of energy generated by the thermal energy and work done by total stress. The fundamental concept of LES is to filter the large and small turbulence scales, where the large scales of turbulence are directly resolved in the flow domain, and the small turbulence eddies are numerically modeled using a subgrid scale (SGS) model. In the present study, the WALE (wall-adapting local eddy viscosity) SGS model was selected, which utilizes a modified form of the velocity gradient tensor, allowing to accurately represent the near-wall behavior of turbulence without requiring any additional damping functions [32]. The SGS eddy viscosity in the WALE model is defined as Eq. (4):

$$\mu_{sgs} = \rho \left(C_w \Delta\right)^2 \frac{\left(S_{ij}^d S_{ij}^d\right)^{3/2}}{\left(\bar{S}_{ij}\bar{S}_{ij}\right)^{5/2} + \left(S_{ij}^d S_{ij}^d\right)^{5/4}} \tag{4}$$

where C_w denotes the WALE constant, Δ is the length scale, and S_{ij}^d is the traceless symmetric part of the square of the velocity gradient tensor.

The SIMPLE algorithm (semi-implicit method for pressure linked equations) was used for the pressure–velocity coupling [33]. For spatial discretization of the convection terms, a bounded central differencing (BCD) scheme was used [34]. This scheme blends the central differencing method with a second-order upwind approach to achieve both accuracy and numerical stability, particularly in regions with strong gradients. An implicit second-order scheme was employed for temporal discretization.

To reduce computational cost, a single-hole model was conducted for the LES simulations, with translational periodic interface boundary conditions applied to the pitchwise domain sides. Air is considered an ideal gas with an inflow velocity of 10 m/s and a temperature of 295 K was set at the mainstream inlet. At the outlet, a static pressure boundary condition corresponding to atmospheric pressure (1 atm) was applied. The plenum chamber inlet was specified with a temperature of 196 K, a turbulence intensity of 1%, and a mass flow rate to match a blowing ratio of 1.5, consistent with experimental conditions [11]. Sutherland's law was used to model the viscosity and temperature-dependent thermal conductivity of the working fluid accurately. Adiabatic and no-slip boundary conditions were set for all walls. To further reduce the computational time, preliminary solutions were obtained using a RANS approach based on the realizable k-ϵ turbulence model. These RANS results served as the initial condition

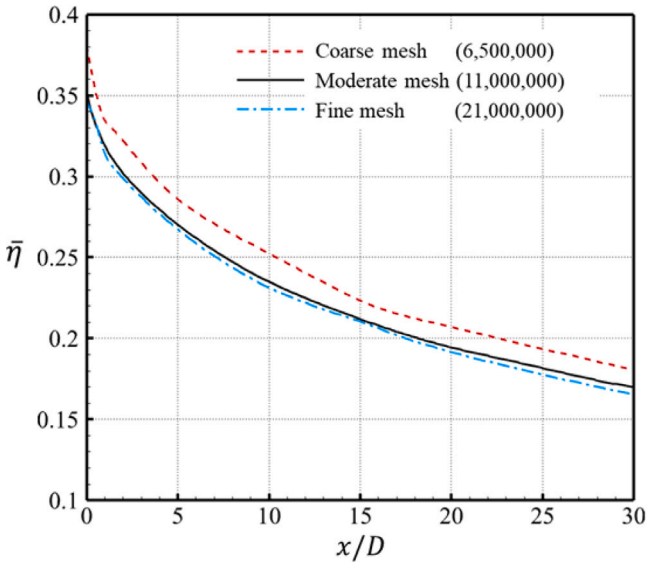

Fig. 4. Grid dependence test.

for subsequent LES simulations. For the LES simulations, a time step of 5 microseconds with 15 inner iterations was selected, ensuring a CFL number below 0.45. To eliminate the influence of the initial RANS solution on the LES results, each LES case was run for approximately five mainstream channel flow-through times. Then, the flow fields were time-averaged over an additional ten flow-through times to capture statistically periodic flow behavior at several monitoring points in the computational domain. All simulations were conducted on the high-performance computing cluster at the University of Bristol using 256 parallel processors. The total computational time for each LES case was approximately 200 h.

2.4. Numerical validation

To evaluate the impact of grid resolution on the predicted film cooling effectiveness, three different mesh resolutions were generated: coarse (6.5 million elements), moderate (11 million elements), and fine (21 million elements). Fig. 4 compares the lateral-averaged film cooling effectiveness ($\bar{\eta}$) profiles computed by the LES approach for the reference case at a fixed density ratio and blowing ratio of 1.5. As shown in the figure, the coarse grid noticeably over-predicts the cooling effectiveness along the streamwise direction when compared to the moderate and fine grids. However, it is observed that by increasing the number of grid points from moderate to fine mesh, there is no significant change in the cooling performance. This suggests that the moderate grid provides a sufficient resolution to capture the heat transfer characteristics near the flat plate surface while maintaining reasonable computational cost. This observation is further supported by the area-averaged cooling effectiveness computed using the LES approach on the flat plate surface for various grid resolutions, as summarized in Table 2. The area-averaged cooling effectiveness was evaluated over a rectangular region on the flat plate, extending 6D in the lateral direction and 30D in the streamwise direction from the trailing edge of the hole. It can be observed that the coarse mesh overpredicts the cooling effectiveness by approximately 11% and 12% compared to the moderate and fine meshes, respectively. In contrast, the area-averaged effectiveness changes only slightly by about 0.6% when refining the grid from the moderate to the fine case.

To validate the accuracy and reliability of the numerical method, the flow field and adiabatic film-cooling effectiveness of the reference cooling hole, computed by the LES approach, were compared with available experimental data [11]. Fig. 5(a) presents the time-averaged normalized velocity contours on the mid-span plane near the hole exit, obtained from LES results and experimental measurements using particle image velocimetry at a density and blowing ratio of 1.5. Good agreement is observed between the LES predictions and experimental data, particularly in terms of the jet penetration characteristics into the mainstream flow, both in pattern and velocity magnitude. Furthermore, Fig. 5(b) compares the streamwise velocity profiles on the centerline plane located at $x/D = -2.3$, measured by laser Doppler velocimetry and computed by the LES approach. The LES method demonstrates a strong capability in predicting the detailed velocity profile, especially in the near wall region ($0 < y/D < 0.4$), where the high-momentum coolant jet significantly alters the local flow structure.

Table 2
Variation of area-averaged cooling effectiveness with different grid resolutions.

Grid resolution	Area-averaged film-cooling effectiveness ($\bar{\eta}$)
Coarse	0.2251
Moderate	0.2028
Fine	0.2010

Fig. 6(a) shows the film cooling effectiveness contours on the flat plate surface for the reference case at a blowing ratio of 1.5, obtained from both experimental measurements [11] and LES results. As illustrated, the LES approach captures the cooling effectiveness distributions with good agreement compared to the experimental data. Additionally, Fig. 6(b) compares the lateral-averaged film cooling effectiveness profiles along the streamwise direction between the LES predictions and experimental results. The LES results closely match the experimental data, demonstrating strong consistency in the streamwise decay and peak effectiveness locations. Figs. 6 and 7 confirm the LES approach's accuracy in capturing the essential flow structures and thermal behavior associated with film cooling, confirming its suitability for detailed analysis of cooling performance.

3. Optimization method

The design variables and objective function were first defined using a preliminary RANS-based study. Subsequently, a design of experiment methodology gave a representative set of samples within the design space. Each of these cases were then evaluated using LES simulation to capture the detailed flow physics accurately, with the resulting objective function values then permitting construction of a surrogate model. This surrogate serves as an efficient approximation of the high-fidelity simulations and allows optimization within the defined design space, however, it is critical that the dimension of this space is not excessive, which motivates the need to have an efficient shape parameterization that can deliver good design space access using a small number of design variables.

3.1. Modal subdivision shape parameterization

Geometric parameterization permits a numerical optimizer to convert from the vector of design variables to the wetted surface required for CFD analysis [35]. It is a key component, the efficacy of which is fundamental in determining how much of the design space is available to the optimizer, as well as the convergence properties of the process in terms of final objective function value and the avoidance of local minima. A good parameterization allows access to a wide range of designs for a small number of design variables, and delivers good final objective function results that are not sensitive to initial starting points or constraints.

Within the context of cooling hole optimization, relatively little is known about the likely optimal shapes, and therefore parameterization flexibility is key to ensuring the design space is adequately explored.

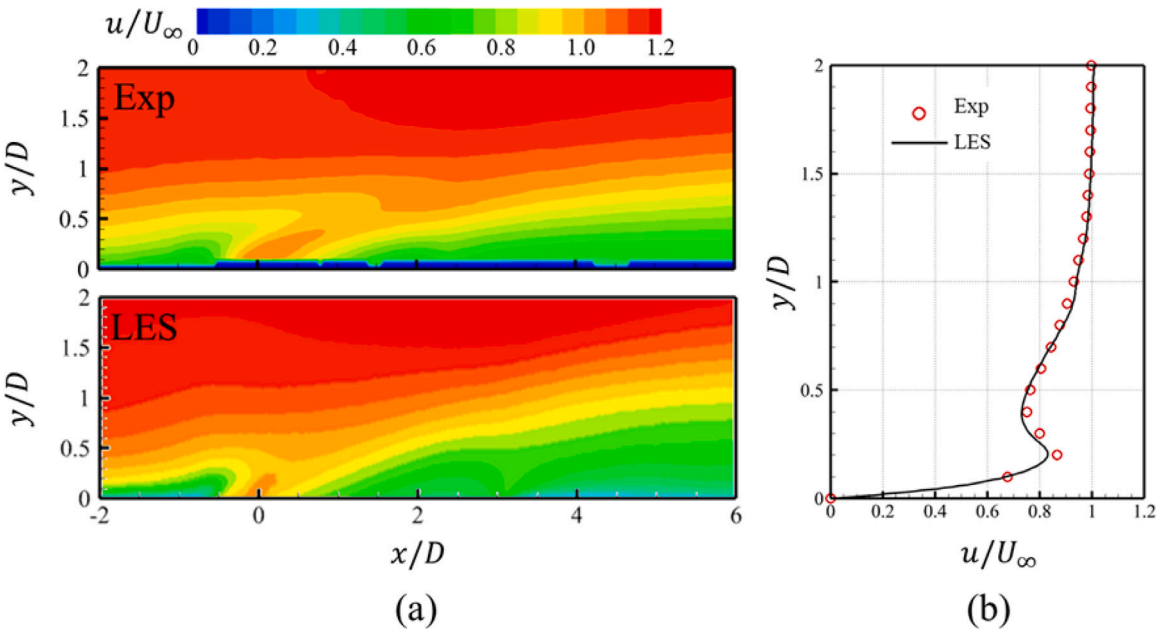

Fig. 5. (a) Time-averaged normalized velocity distribution on the mid-span plane, measured using PIV technique [11] and computed by the LES approach for the reference case, (b) velocity profiles measured using laser Doppler velocimetry [11] and computed by the LES approach at $x/D = -2.3$ in the streamwise direction.

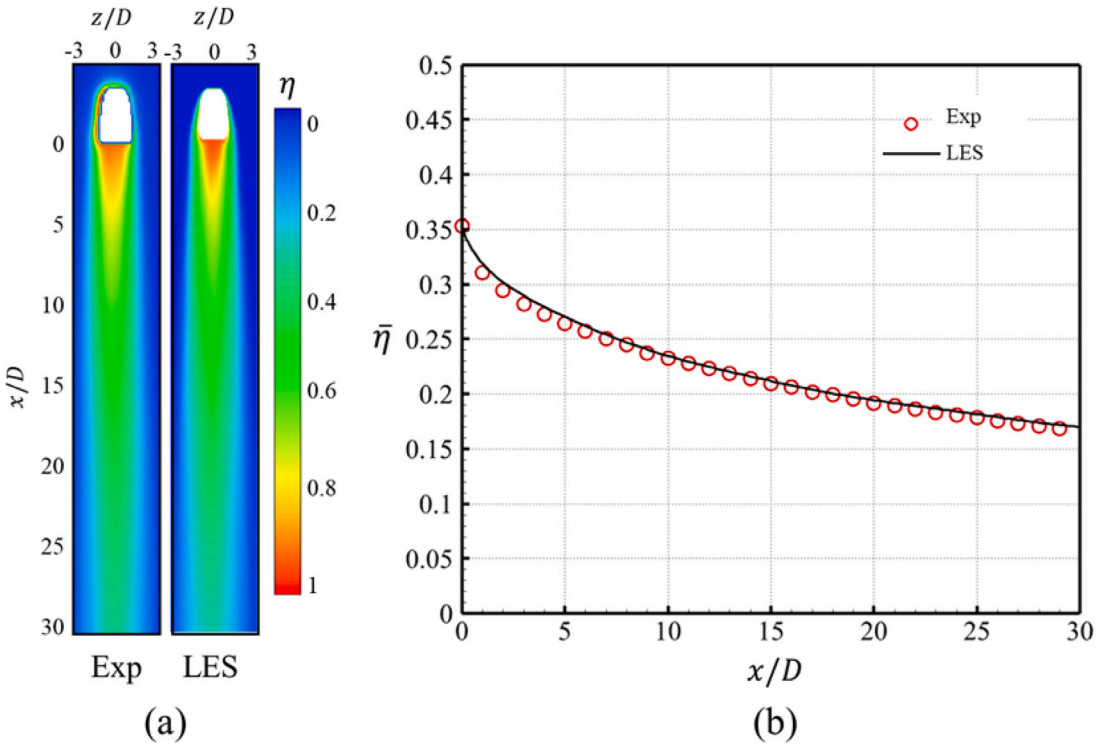

Fig. 6. Time-averaged film-cooling effectiveness distribution measured by experiment [11] and computed by the LES approach for the reference case: (a) film-cooling effectiveness contour on the flat plate surface, (b) lateral-averaged film-cooling effectiveness along the streamwise direction.

This is in contrast to, for example, airfoil or wing optimization where parameterizations are readily available but often tailored to those specific geometries [35]. Prior cooling hole design has explored common parameterizations that include radii, angle and lengths [20–22,31], but these unreasonably limit the palette available to the numerical procedure and constrain results to conform to what practitioners perceive might be beneficial, rather than leaving this open to the optimization to resolve.

One parameterization method involves using subdivision surfaces [36] (commonly used in computer animation), whereby the control point motions permit geometric changes to be propagated through to the final limit surface. This has been successful in matching or exceeding airfoil-specific methods while remaining generally applicable to any surface, and also supports hierarchical optimization [37]. However, for the surrogate process used here, and given the high cost of LES modeling, an alternative approach is warranted to simplify the design

space further without compromising the geometrics flexibility. It would be unreasonably costly to explore the high dimensional design space generated by full control point motions for a subdivision scheme, which motivates finding a much smaller design space based on an orthogonal decomposition of that space.

In this work, rather then employing subdivision control points directly [38], a set of design vectors is derived through a singular value decomposition of the subdivision limit matrix for an initial surface mesh [37]. These design vectors can then be summed with the coordinate positions of the initial surface mesh. Each vector applies global, wave-like deformations to the surface of different frequencies. Subdivision is a mesh smoothing and refinement algorithm which defines a limit surface from a coarse surface mesh through a process of recursive refinement [36,39]. The process works on the basis of inserting additional surface nodes alongside those that already exist in the surface mesh, before a smoothing operation is applied over all nodes. This process and applied recursively, but it is also possible to calculate the final, limit position of any node on the surface. These limit positions of each of the surface mesh vertices can also be calculated as an average of its coordinates and the coordinates of its surrounding vertices [40]. This allows a matrix multiplication to be written which maps each point on the initial surface to its limit position

$$C_\infty = \mathbf{L}C_0 \tag{5}$$

where C_0 gives the initial coordinates of the surface mesh and C_∞ gives the coordinates of the limit position of the same points. The limit matrix, $\mathbf{L}$, is a sparse matrix which contains adjacency information with smoothing properties. It is this limit matrix that is suitable for singular value decomposition, and therefore the subdivision control points themselves are not used directly here; rather, the connectivity information present in the subdivision scheme is used for construction of the orthogonal space.

The singular value decomposition of this sparse matrix gives

$$\mathbf{L} = \mathbf{USV}^* \tag{6}$$

where $\mathbf{U}$ is a matrix whose columns are an orthogonal basis in the row space of $\mathbf{L}$; $\mathbf{S}$ is a diagonal matrix of singular values; and $\mathbf{V}^*$ is the conjugate transpose of $\mathbf{V}$, a matrix whose columns are an orthogonal basis in the row space of $\mathbf{L}$. The columns of $\mathbf{U}$ can be used as a set of orthogonal design vectors of increasing frequency which can be scaled with an amplitude and summed with the surface mesh coordinates to apply smooth deformations. These design vectors can be defined as the modes. For reference, mode numbers can be given to the successive columns.

In summary, using a design of experiment approach necessitates a small number of design variables. Geometrically orthogonal modes give an efficient coverage of spatial deformations, and the matrix system that a subdivision surface scheme produces is highly amenable to this type of decomposition. Even after a compact decomposition of this type, it is still necessary to select those modal deformations that might be anticipated to provide the greatest benefits, with the lowest frequency shapes likely being the most attractive for this purpose.

3.2. Design of experiment method

As illustrated in Fig. 2, two important geometric parameters of the cooling hole surface, the mode number and mode amplitude, are selected as the design variables for the optimization process. In this study, only the surface of the diffuser section of the laidback fan-shape cooling hole was modified, while the metering section and hole exit area were kept unchanged to isolate the effects of diffuser geometry on film cooling performance. The blowing ratio ($M = 1.5$) and density ratio ($DR = 1.5$), were maintained constant throughout all simulations to ensure consistent operating conditions. The primary objective of this study is to enhance the cooling effectiveness by optimizing the surface contour of the diffuser section. Therefore, the area-averaged cooling effectiveness was adopted as the objective function for the optimization algorithm. Table 3 summarizes the lower and upper bounds for the design variables, which were selected to constrain the experiment to physical shapes with no intersections.

Table 3
The design variables for design of experiment method.

Design variable	Lower bound	Upper bound
Mode number (N)	1	8
Mode amplitude (A)	$-0.175D$	$0.175D$

Table 4
LHS designed cases.

Case	Mode number (N)	Mode amplitude (A/D)
Reference	–	–
Case1	1	−0.025
Case2	2	0.125
Case3	3	−0.125
Case4	4	0.025
Case5	5	0.175
Case6	6	−0.175
Case7	7	0.075
Case8	8	−0.075

The DOE technique is a statistical method used to determine representative sampling cases while minimizing the total number of required simulations or tests. In this study, the Latin Hypercube sampling (LHS) approach, originally introduced by McKay et al. [41], was employed to generate the sampling configurations. The LHS method enhances the Monte Carlo technique, ensuring that samples are uniformly distributed across the domain without repetition, which leads to a reduction in number of generated samples. In the current study, eight sampling cases were generated using the LHS DOE method and evaluated by the LES approach, as detailed in Table 4. Fig. 7 presents the schematic view of eight representative cooling hole geometries, highlighting the cutting edges on the mid-span plane for each of the selected sampling cases. It can be observed that the surface geometry of the diffuser sections of the cooling holes exhibits noticeable variations with a wavy pattern, introduced by the shape modal parameterization technique.

After conducting LES simulations for the designed cases, a response surface methodology (RSM) was employed to statistically relate the objective function to the design variables. In the present study, a genetic aggregation (GA) technique [42] was utilized to construct a surrogate model capable of accurately capturing the system's response characteristics. The GA method constructs an ensemble-based surrogate model by defining a weighted average of multiple response surface models. The optimal set of weighting factors is determined by minimizing the root mean square error at the design points. Once the surrogate model was established using the GA method, a multi-objective genetic algorithm (MOGA) [42], an iterative algorithm that supports all types of input variables, was used as the optimization algorithm to identify optimal design parameters.

4. Results and discussions

4.1. Impact of design parameters on cooling performance

Fig. 8 presents the distributions of time-averaged film-cooling effectiveness computed by the LES approach for both the reference and selected sampling cases on the flat plate surface at $M = 1.5$ and $DR = 1.5$. The results indicate that both the magnitude and spatial distribution of the coolant are significantly influenced by modifications to the diffuser section geometry of the cooling hole. Specifically, the application of shape modal variations on the internal surface of the diffuser section leads to a notable downstream extension of the film coolant coverage compared to the reference hole. As shown in Fig. 8, all

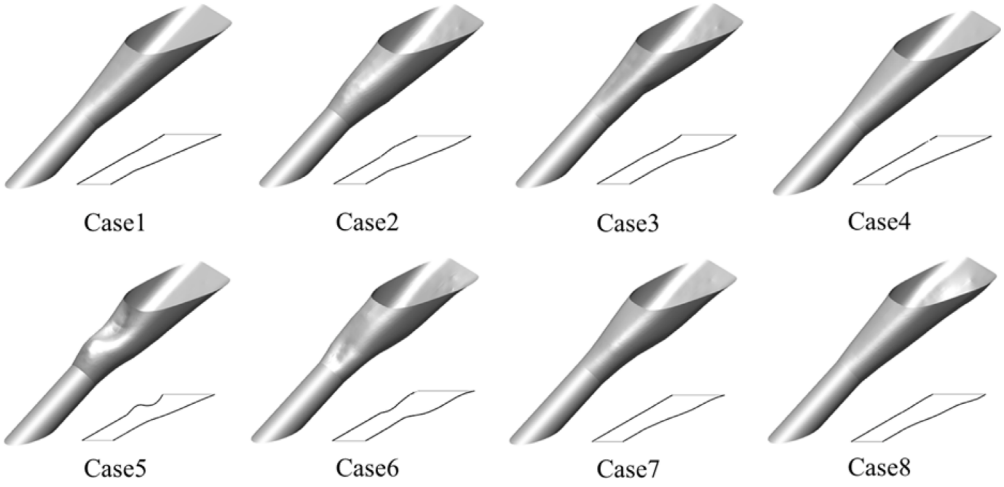

Fig. 7. Schematic view of sampling cases generated by the LHS method.

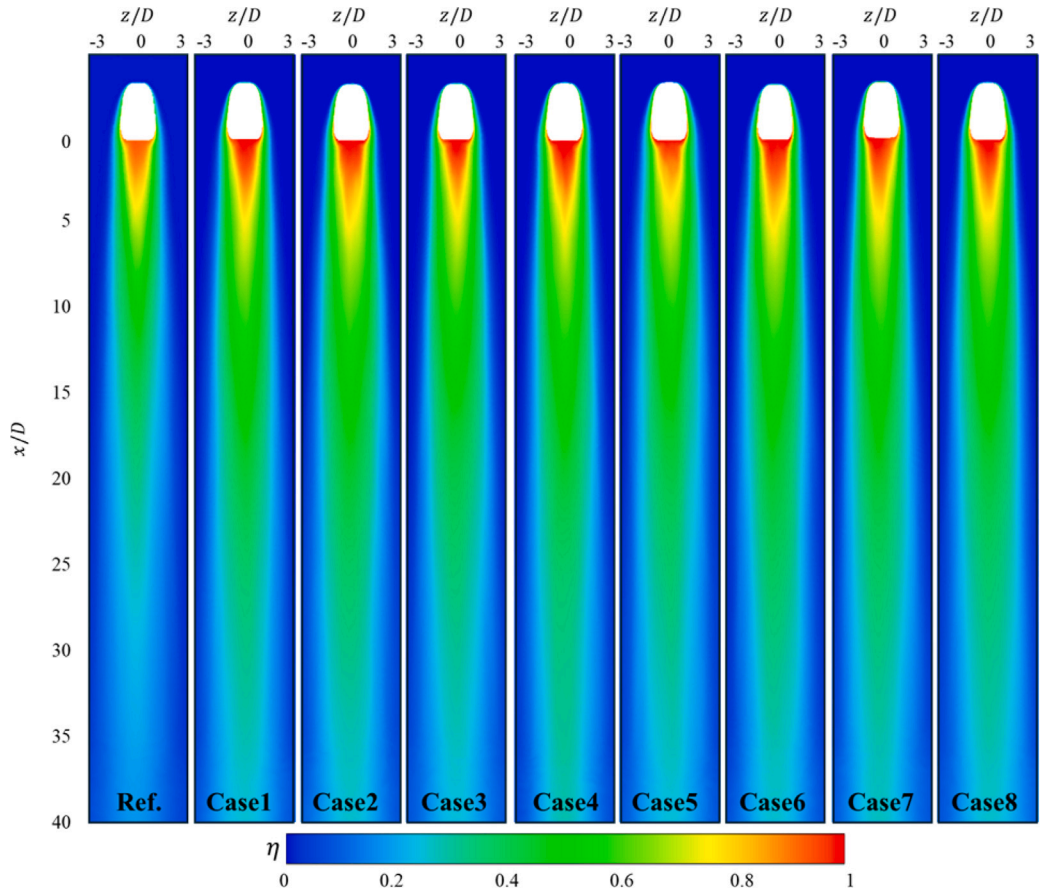

Fig. 8. Distributions of time-averaged film-cooling effectiveness calculated by the LES approach on the flat plate for the reference and designed cases at M = 1.5.

designed cases exhibit an increase in film cooling effectiveness near the hole exit relative to the reference case. Furthermore, lateral spreading of the coolant on the flat plate surface is enhanced, particularly in Case2, Case6, Case7 and Case8. These cases feature outward dilation of leeward-side surface of the diffuser, as previously illustrated in Fig. 7. This geometric alteration modifies the flow structure within the hole, especially the separation bubble near the leeward surface, which plays a critical role in determining the coolant trajectory, surface coverage, and the nature of coolant–mainstream interactions in shaped cooling holes.

Fig. 9 presents a comparison of $\bar{\eta}$ profiles computed by the LES approach for the reference case and several designed cases. Note that the experimentally measured lateral-averaged cooling effectiveness profile [11] is also included. It is evident that all the designed cases show a significant enhancement in lateral coolant coverage along the streamwise direction, particularly within the range of $0 < x/D < 10$, which aligns well with the cooling effectiveness distributions illustrated in Fig. 8. Among the various cases, Case6 and Case8 demonstrate superior film cooling performance in the lateral direction, indicating improved coolant spreading and surface protection.

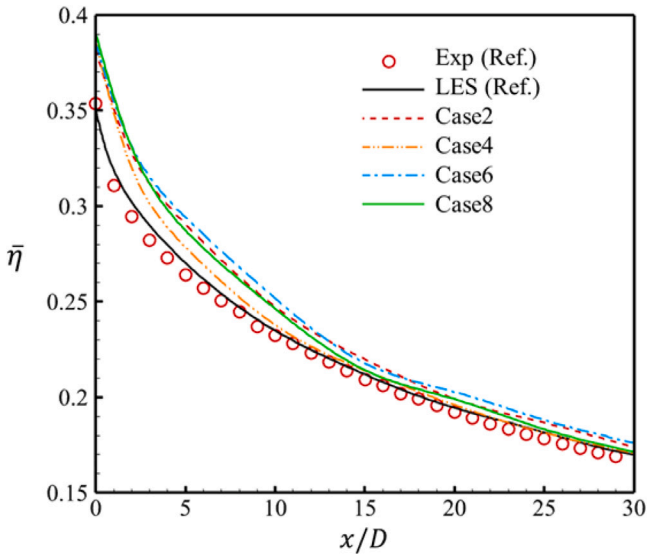

Fig. 9. Lateral-averaged film cooling effectiveness profiles computed using the LES approach on the flat plate for the reference and various designed cases at $M = 1.5$.

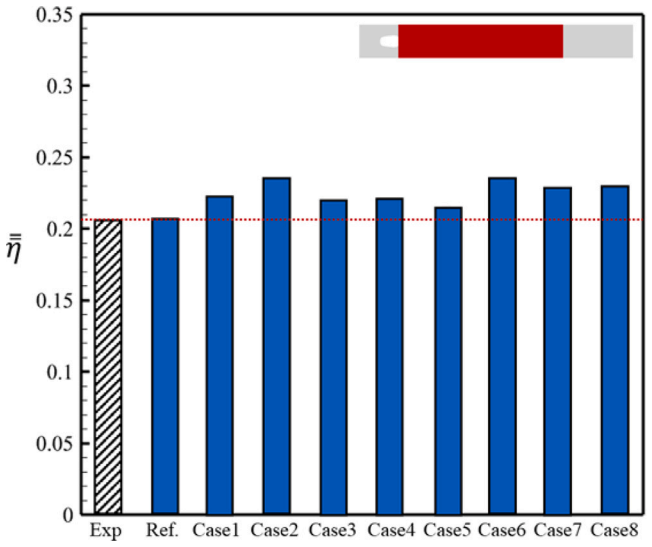

Fig. 10. Overall area-averaged film cooling effectiveness computed by the LES approach on the flat plate for the reference and designed cases.

To evaluate the overall impact of cooling hole surface modifications on cooling performance, the area-averaged cooling effectiveness computed by the LES approach for various designed cases is compared with that of the reference cooling hole at a blowing ratio of 1.5, as shown in Fig. 10. As shown in Fig. 10, all the designed cases demonstrate an improvement in area-averaged cooling effectiveness relative to the reference configuration. Among the designed cases, while Case5 shows the lowest cooling effectiveness, it achieves approximately 4% higher than the reference hole. Case6 shows the highest cooling performance, with an enhancement of approximately 17% over the baseline case. This was caused by the enlarged cross-sectional area on both the leeward and windward sides of the hole. The enlargement in the diffuse section reduces the coolant jet momentum, particularly near the windward side, allowing the low-momentum jet to reach the hole exit and interact with the hot mainstream flow. Consequently, the mixing between the jet and the mainstream is reduced, and the jet penetration into the mainstream is weakened, thereby enhancing the overall cooling performance.

Fig. 11 presents the instantaneous dimensionless temperature (θ) contour obtained using the LES approach on the mid-span cutting plane for reference and designed cases. The temperature is normalized using the mainstream and coolant temperatures. As shown in Fig. 11, the interaction between the coolant jet and the mainstream flow induces complex unsteady structures at the cooling hole exit, known as Kelvin–Helmholtz instabilities. Although the overall temperature distribution patterns are generally similar between the reference and the designed cooling holes, the designed cases show a more extended high-intensity coolant penetration along the streamwise direction, particularly evident in the pink-colored regions of the contours. A comparison of the dark blue color regions adjacent to the surface, indicating lower temperatures and thus better cooling effectiveness, reveals that Case2, Case6, Case7, and Case8 outperform the others. This improvement can be attributed to modifications on the leeward side of the diffuser surface, which alter the separation bubble configuration and enhance coolant jet attachment and spreading.

To investigate the influence of cooling hole surface geometry on film-cooling performance along the streamwise direction, Fig. 12 compares the time-averaged, dimensionless temperature fields calculated by the LES approach for the reference hole, Case5 (the lowest cooling performance among the designed cases), and Case6 (the highest cooling performance among the designed cases) on three streamwise cross-sectional planes located at $x/D = 0$, 5, and 10. It should be noted that both the x and y axes are normalized by the cooling hole diameter. Across all cases, increasing x/D results in a reduction of cooling effectiveness and a broader spread of the coolant in the wall-normal direction. At $x/D = 0$, the coolant distribution for both designed cases extends more in the lateral direction and remains concentrated closer to the surface and hole exit, leading to improved cooling performance relative to the reference case. In contrast, the reference cooling hole shows a greater vertical extension up to $y/D = 1$, indicating more significant jet lift-off and less effective surface coverage. At $x/D = 5$, both Case5 and Case6 demonstrate improved coolant effectiveness compared to the reference case. At $x/D = 10$, only Case6 maintains a notable low-temperature region (depicted in blue in Fig. 12), consistent with the results shown in Figs. 8 and 11.

4.2. Impact of design parameters on flow structure

Fig. 13 presents the normalized time-averaged velocity magnitude computed by the LES method on the mid-span plane for the reference and designed cases. The velocity magnitude is normalized by the freestream velocity (10 m/s). As shown in Fig. 13, alterations in the diffuser surface geometry significantly affect the coolant jet behavior and the structure of the separation bubbles within the cooling holes. For all designed cases, a reduction in jet momentum at the hole exit is observed compared to the reference case. This reduction is primarily attributed to variation in the cross-sectional area of the diffuser section, which enhances the film cooling efficiency by promoting a more favorable jet trajectory. Case5, characterized by the largest outward modal amplitude deformation, exhibits a pronounced cavity-like formation on the windward side of the hole. This change further diminishes the jet momentum and reduces the size of the internal separation bubble relative to the other designed cases. Despite demonstrating improved cooling efficiency over the baseline hole, Case5 shows the lowest film-cooling effectiveness among all the designed cases. This finding indicates that jet momentum and separation bubble positioning within the shaped cooling hole play important roles in determining the interaction between the coolant jet and the mainstream flows, thereby influencing overall cooling performance.

To better understand the impact of surface modifications of the cooling hole on flow structures within the hole, Fig. 14 shows the instantaneous distributions of the normalized z-component of vorticity

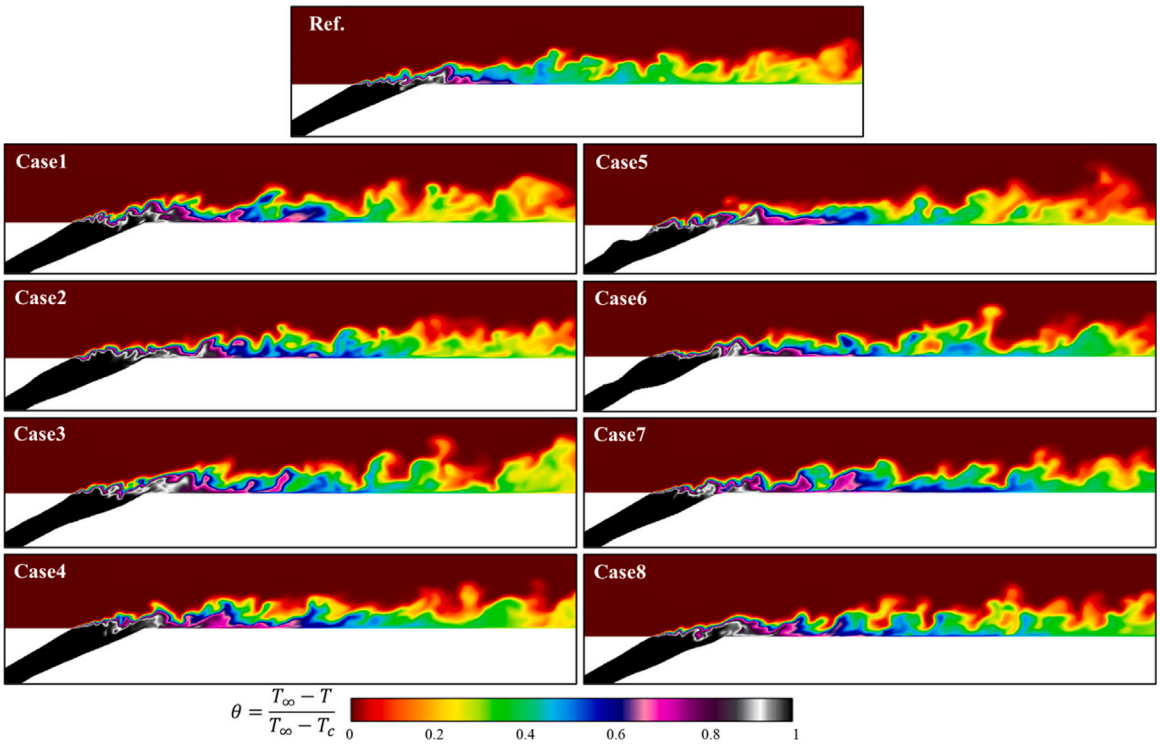

Fig. 11. Instantaneous non-dimensional temperature distributions on the mid-span plane for the reference and designed cases.

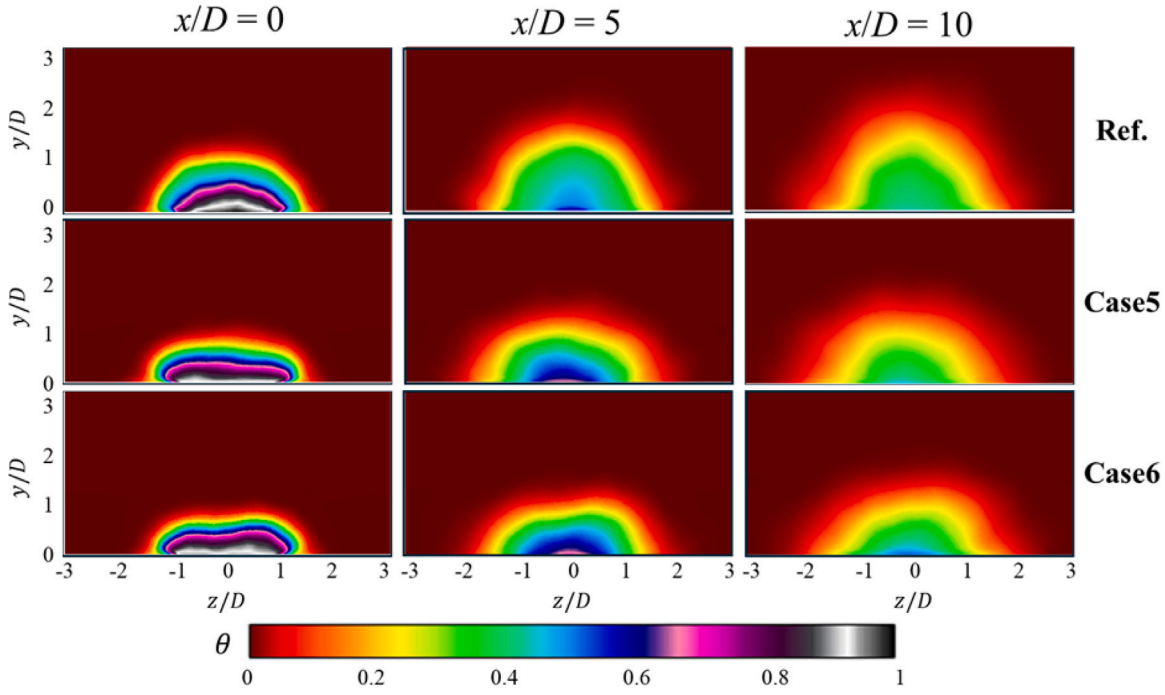

Fig. 12. Time-averaged, dimensionless temperature distributions calculated by the LES approach for the reference case, Case5, and Case6 on cross-planes located at x/D = 0, 5, and 10.

on the mid-span plane for the baseline configuration, Case5 and Case6. The vorticity is non-dimensionalized using the hole diameter (D) and the freestream velocity (U_∞). As shown in Fig. 14, periodic clockwise vortical structures (represented by dark blue regions in the figure) are generated at the inlet of the cooling hole due to entrance effects and are subsequently convected downstream through the metering and diffuser sections. In the reference hole, these vortical structures are directed toward the windward side of the hole and are extended toward the hole exit, interacting with the mainstream flow. In contrast, in the modified geometries (Case5 and Case6), the altered diffuser surfaces significantly affect the internal flow structures. In these cases, the initial vortices are disrupted and interact with additional vortical motions generated within the diffuser section, preventing them from persisting to the hole exit. In Case5, the cavity-like feature on the windward side promotes the formation of a prominent counter-clockwise vortex (dark red region highlighted by ①), which redirects the coolant jet toward

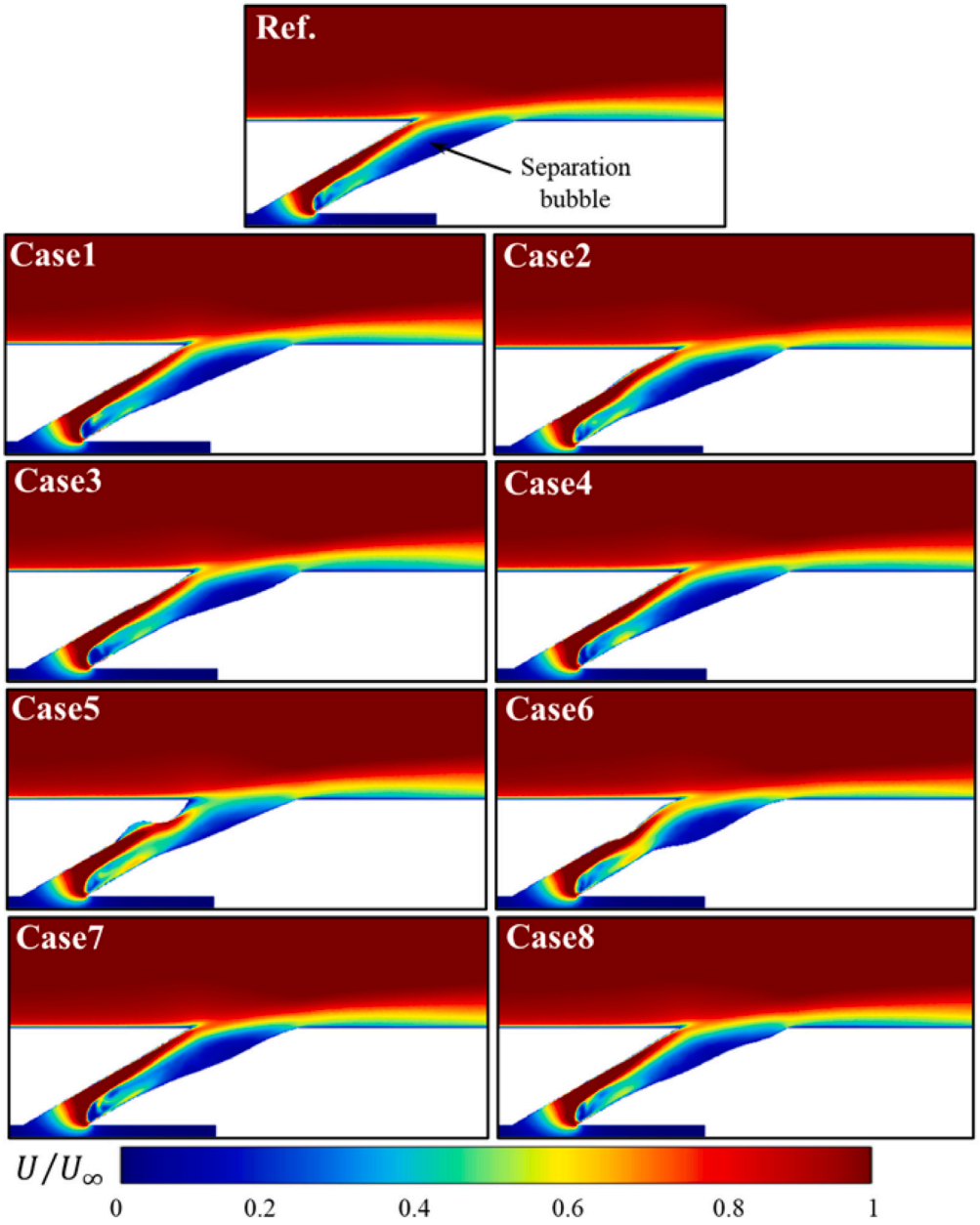

Fig. 13. Time-averaged, normalized velocity magnitude distributions calculated by the LES approach for the reference and designed cases on mid-span plane.

the windward side. However, the subsequent inward bump on the same side (indicated by ②) acts as a partial flow obstruction, diminishing the jet's momentum and altering its exit trajectory. For Case6, outward expansion on both the windward and leeward sides facilitate a broader flow path, pushing the coolant jet toward the windward side. This geometric configuration results in earlier interaction between the coolant and mainstream, particularly near the leading edge at the hole exit.

To investigate the impact of diffuser surface modifications on the turbulence characteristics of the coolant jet, the time-averaged, normalized turbulence kinetic energy (TKE) computed by the LES approach for the reference hole, Case5 and Case6 is shown on the mid-span plane in Fig. 15. The TKE values are normalized by the square of the freestream velocity. TKE represents the mean kinetic energy associated with turbulent eddies, which affects the development and dispersion of the coolant jet as it exits the cooling hole and interacts with the high-temperature mainstream flow. As shown in Fig. 15, the magnitude of the high TKE region within the cooling hole is noticeably reduced in the modified geometries (Case5 and Case6) compared to the reference case. In the reference case, a high TKE region originates in the diffuser section of the hole and extends toward the windward side at the hole exit. In contrast, the designed cases confine this high TKE region mostly within the diffuser section, preventing it from reaching the hole exit. This reduction of turbulence intensity in the designed cases contributes to a reduction in the jet's momentum, thereby weakening the mixing between the coolant and mainstream flows. As a result, the coolant jet exhibits reduced penetration into the mainstream and remains more closely attached to the surface, enhancing surface coverage, as shown in Fig. 10. It is interesting to note that, in Case5, an additional high TKE region appears within a cavity-like structure inside the cooling hole. This localized turbulence intensification further reduces the jet's momentum and increases the flow unsteadiness within the diffuser, leading to a decline in film cooling effectiveness relative to Case6.

Figs. 16(a) and (b) present a comparison of the instantaneous iso-surfaces of the $Q_{Criterion}$ for the reference hole and Case6, respectively. The $Q_{Criterion}$, set to a constant value of 350,000 s^{-2}, is commonly used to visualize coherent vortical structures and assess the impact of

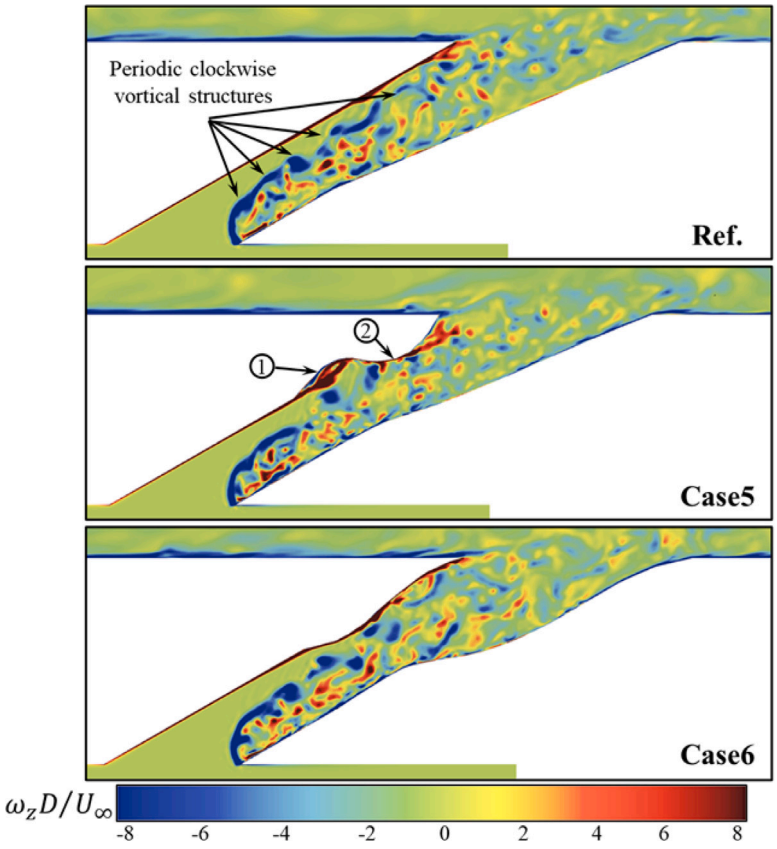

Fig. 14. Instantaneous distributions of the normalized z-component of vorticity on the mid-span plane for the baseline configuration, Case5 and Case6.

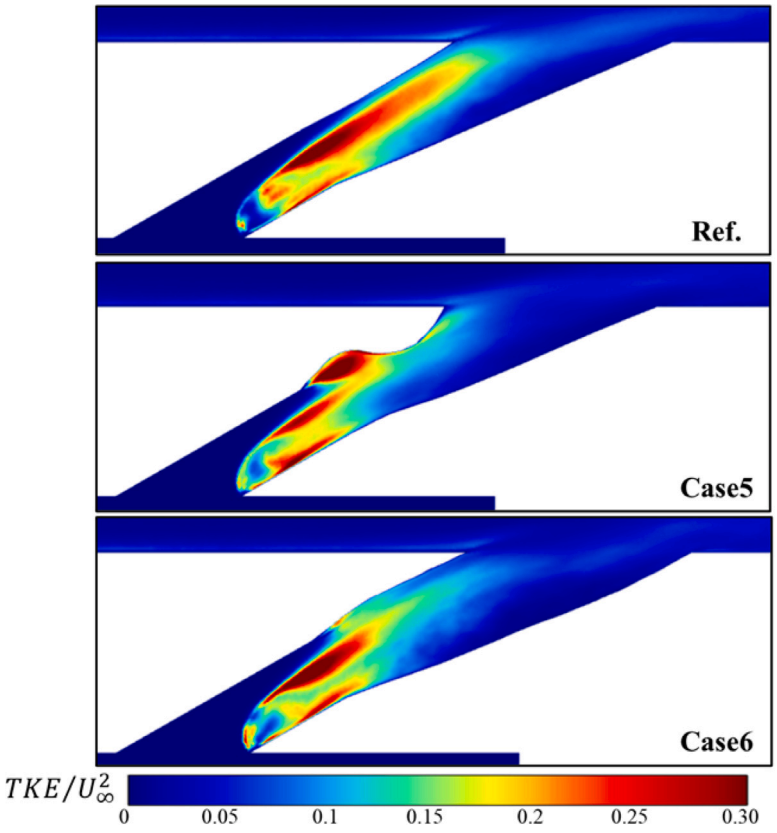

Fig. 15. Distributions of time-averaged normalized turbulence kinetic energy computed by the LES approach on the mid-span plane for the baseline configuration, Case5 and Case6.

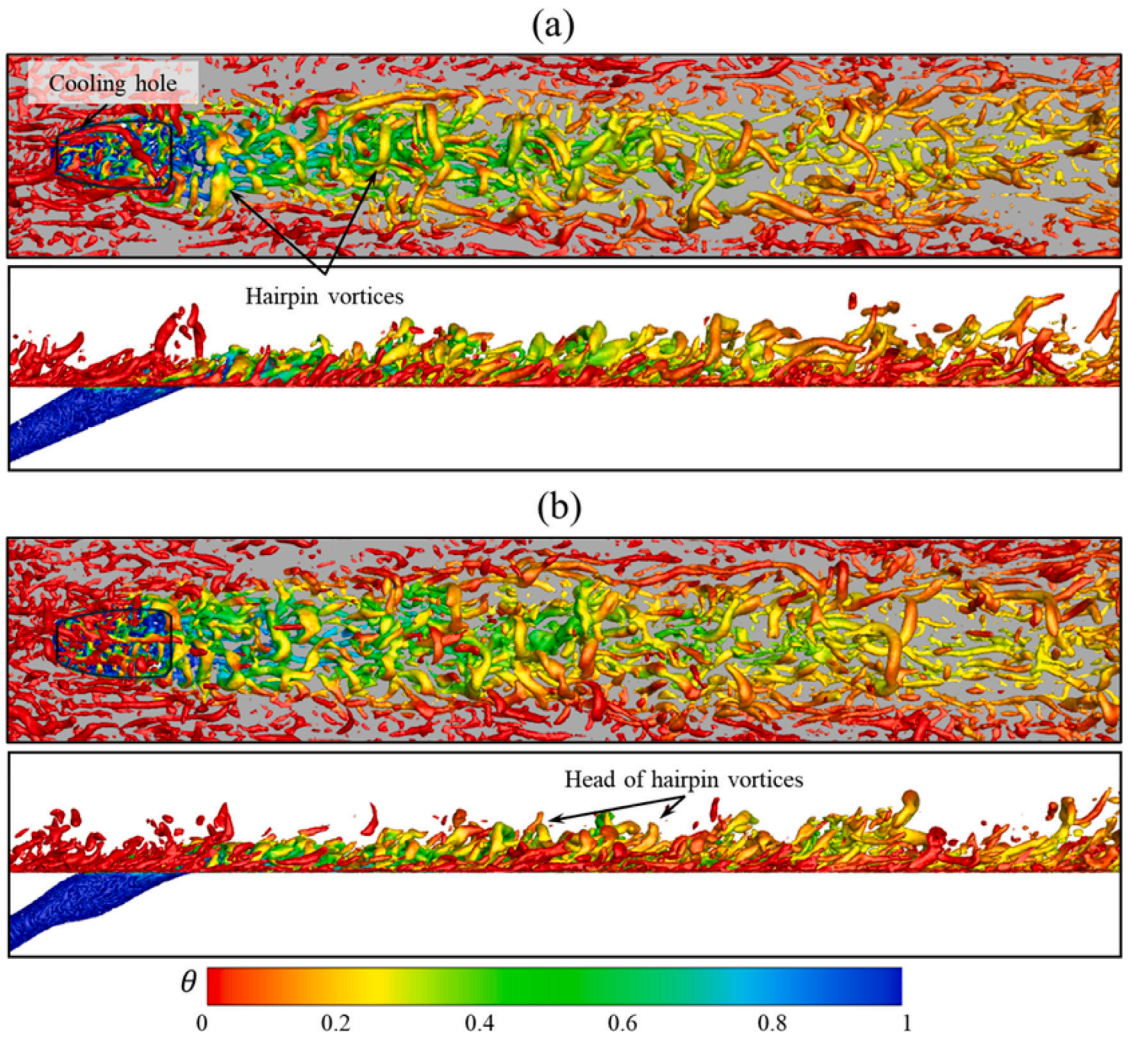

Fig. 16. Instantaneous iso-surface of $Q_{Criterion}$ colored by the non-dimensional temperature over the flat plate surface: (a) reference hole, (b) Case6.

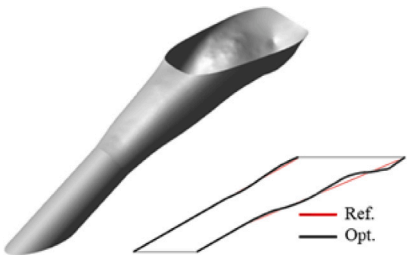

Fig. 17. Schematic view of the optimized cooling hole configuration.

geometric modifications to the cooling hole on flow behavior over the flat plate. Note that the iso-surfaces are colored by the instantaneous, non-dimensional temperature field. As shown in Fig. 16, the tripping wire upstream of the coolant injection effectively induces a turbulent boundary layer, which plays a crucial role in enhancing the interaction between the main flow and the coolant jet. The hairpin vortices are generated at the cooling hole exit and are convected downstream. These vortical structures are extended in both the lateral and normal directions, generating a pair of counter-rotating vortices between their legs, which are important factors in maintaining the coolant close to the surface. A comparative analysis of Figs. 16(a) and (b) indicates that Case6 generates a higher number of hairpin vortices, with greater lateral extension. This enhanced vortex generation improves coolant dispersion and surface coverage. In contrast, the reference hole configuration exhibits larger hairpin vortices that are more elongated in the normal direction, as evident in the side-view figures in Fig. 16. This behavior is attributed to the higher momentum of the coolant jet at the exit, leading to increased jet lift-off and consequently, a reduction in surface cooling effectiveness.

4.3. Cooling hole optimal configuration

The LES results obtained from eight different designed cases were utilized to optimize the surface geometry for enhanced film-cooling performance. As discussed in Section 3.2, variations in modal number and amplitude were introduced to maximize the area-averaged film-cooling effectiveness. A GA algorithm was applied to construct a surrogate response surface model, while a MOGA algorithm was used to identify the optimal design parameters. The optimal values of the design variables, along with the corresponding cooling effectiveness computed by the LES approach and predicted by MOGA method, are presented in Table 5. The discrepancy between the LES-computed and MOGA-predicted optimal film-cooling effectiveness was approximately 0.6%, demonstrating the reliability and predictive capability of the LES-based optimization framework for determining the most effective cooling hole configuration.

Fig. 17 shows a schematic illustration of the optimized cooling hole geometry and its mid-span plane profile, compared with that of the baseline hole. The geometry reveals an outward expansion on the

Table 5
LES-based optimization results.

Case	Design variables		Objective function	
	Mode number (N)	Mode amplitude (A)	MOGA prediction	LES
Reference	–	–	–	0.2028
Optimal	8	$-0.154D$	0.2491	0.2475

windward side of the hole, while the diffuser region near the exit exhibits an inward protrusion resembling the characteristic shape of trenched cooling hole configurations [8,17].

Fig. 18(a) compares the time-averaged film-cooling effectiveness distributions, computed by the LES approach, on the flat plate surface for both the reference and optimized cooling hole configurations. In the case of the optimized hole, a notable enhancement in cooling performance is observed near the hole exit, corresponding to the red region in the figure, with the high-effectiveness region extending further downstream up to $x/D \approx 5$. Additionally, the lateral spread of the coolant is wider compared to that of the reference hole, indicating improved lateral coolant coverage. Fig. 18(b) shows the lateral-averaged film cooling effectiveness for both cases. Across the entire x/D range, the optimized hole demonstrates superior cooling performance relative to the reference case. As quantitatively summarized in Table 5, the overall cooling performance of the optimized hole exhibits an improvement of approximately 22% compared to the reference case.

Figs. 19(a) and (b) present the instantaneous and time-averaged normalized temperature distributions, respectively, obtained using the LES approach across multiple cutting planes for the optimized cooling hole configuration. A comparison between Figs. 11 and 19(a) reveals a marked improvement in the instantaneous temperature field at the mid-span plane for the optimized geometry. This enhancement is particularly evident in the gray color region near the hole exit in Fig. 19(a), which extends further downstream along the flat plate surface, indicating a more effective thermal coverage and improved cooling behavior. Furthermore, Fig. 19(b) demonstrates that the time-averaged temperature distribution near the wall is also improved relative to the reference case depicted in Fig. 12. Across all x/D cross-sectional planes, the optimized hole configuration shows superior thermal performance, maintaining higher normalized temperatures and thus better cooling effectiveness. Notably, it even exceeds the performance of the best-performing design among the evaluated designed cases (Case6), highlighting the success of the optimization strategy.

Figs. 20(a) and (b) present the time-averaged normalized velocity and TKE distributions within the optimized cooling hole along the mid-span cutting plane. As shown in Fig. 20(a), the coolant jet remains attached to the windward side wall up to the exit of the cooling hole. This attachment facilitates an earlier and more directed interaction between the jet and the mainstream flows, thereby enhancing the local cooling performance [43]. Furthermore, the presence of a trench-like feature near the trailing edge of the hole enlarges the separation bubble within the diffuser region. This geometric modification promotes a lateral deflection of the coolant jet toward the windward side, contributing to a more favorable flow structure for film cooling. A comparison of the TKE distributions shown in Fig. 20(b) for the optimized hole with those of the reference and designed cases (as seen Fig. 15) reveals a noticeable reduction in TKE, particularly near the interface between the metering section and diffuser. This reduction indicates diminished unsteadiness and lower turbulence intensities within the hole. As a result, the turbulence convected through the hole exit is also reduced, leading to a weaker jet-mainstream interaction and consequently less turbulence mixing. Such flow behavior is beneficial for maintaining a coherent coolant film along the surface downstream of the hole.

Fig. 21 presents a comparison of time-averaged, normalized velocity magnitude distributions between the reference and optimized cooling hole configurations at four streamwise cross-sectional planes along the centerline (L/D = 1.5, 2.5, 3.5, and 4.5). At L/D = 1.5, the flow structures predicted by the LES method are similar for both cases. A low-momentum (separated) region appears near the leeward side of the

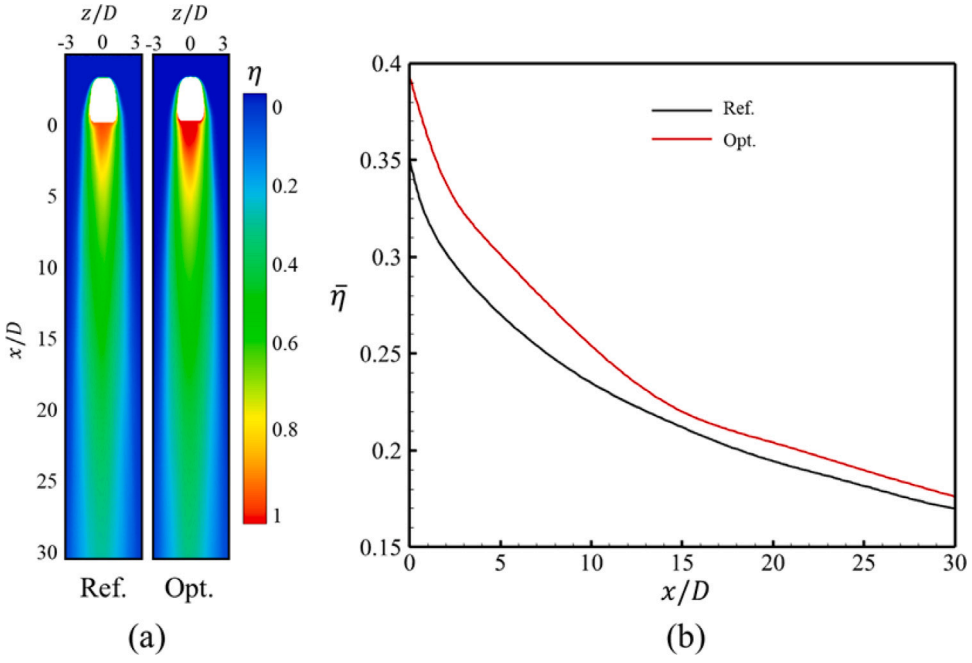

Fig. 18. Comparison of the cooling performance between the reference and optimized holes: (a) time-averaged cooling effectiveness distributions, (b) lateral-averaged cooling effectiveness.

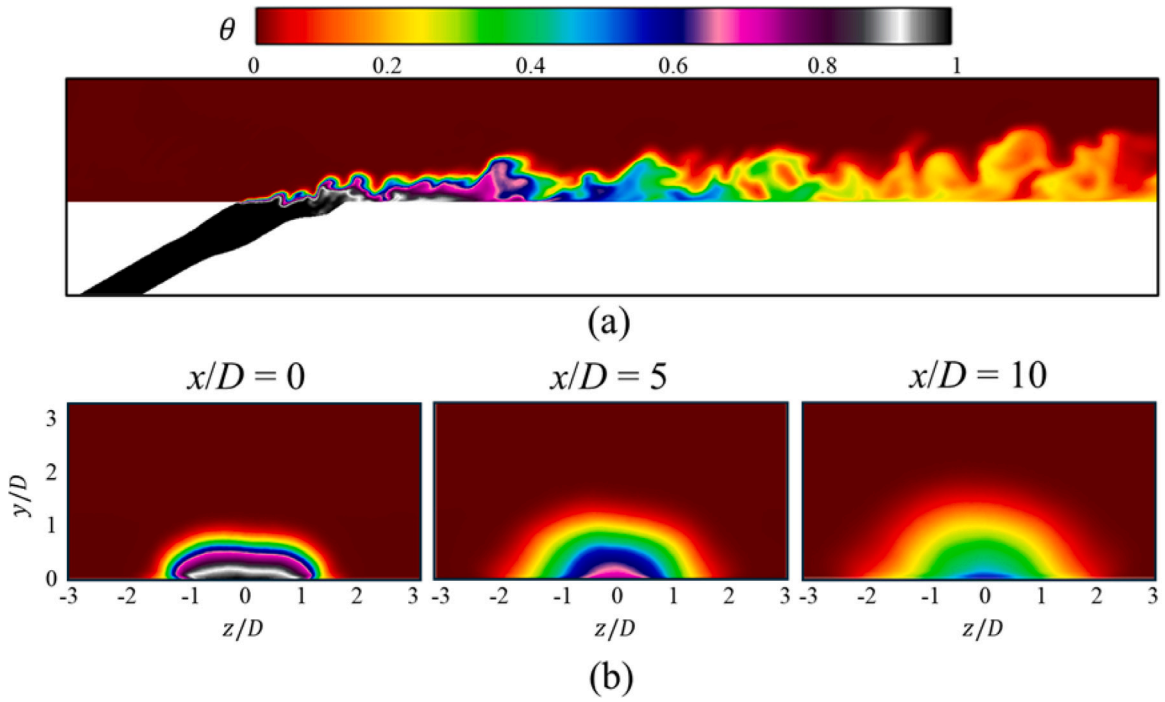

Fig. 19. Distributions of the normalized temperature for the optimized hole: (a) instantaneous distribution on the mid-span plane, (b) time-averaged distribution on the cross-planes located at x/D =0, 5, and 10.

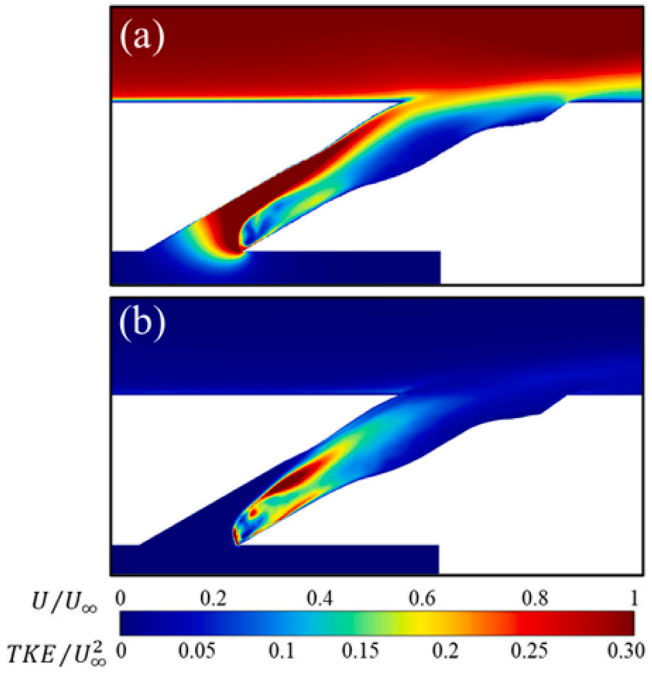

Fig. 20. Distributions of time-averaged flow fields within the optimized hole on the mid-span plane: (a) velocity magnitude, (b) turbulence kinetic energy (TKE) magnitude.

metering section, attributed to the entrance effect of the cooling hole. The high-velocity region, corresponding to the coolant jet, is primarily directed toward the windward side. At L/D = 2.5, the optimized

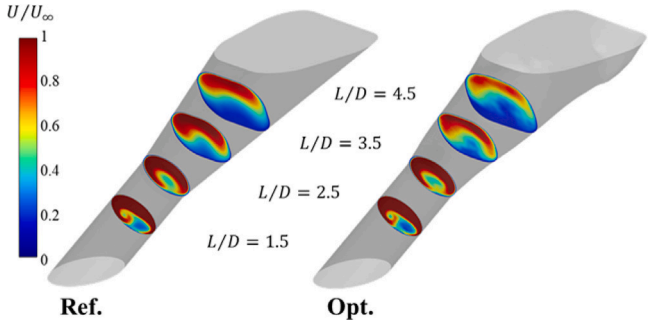

Fig. 21. Distributions of time-averaged normalized velocity magnitude for the reference and optimized cooling holes at streamwise planes located at L/D = 1.5, 2.5, 3.5, and 4.5.

hole exhibits an expanded low-velocity region to the reference case, indicating the development of a larger separation bubble along the leeward surface of the diffuser section. As L/D increases to 3.5 and 4.5, the low-velocity region (depicted in blue) becomes more pronounced in the optimized configuration, accompanied by a noticeable reduction in jet momentum compared to the reference hole. This decrease in momentum contributes to lower turbulence intensity and improved cooling effectiveness, which is consistent with the TKE distributions shown in Fig. 20(b).

4.4. Analysis of temporal/spatial characteristics

Since cooling hole surface geometry significantly affects the cooling effectiveness, a time/space analysis is conducted to evaluate the flow characteristics and unsteady phenomena both inside the hole and in the mixing region downstream of the hole exit. Fig. 22 illustrates

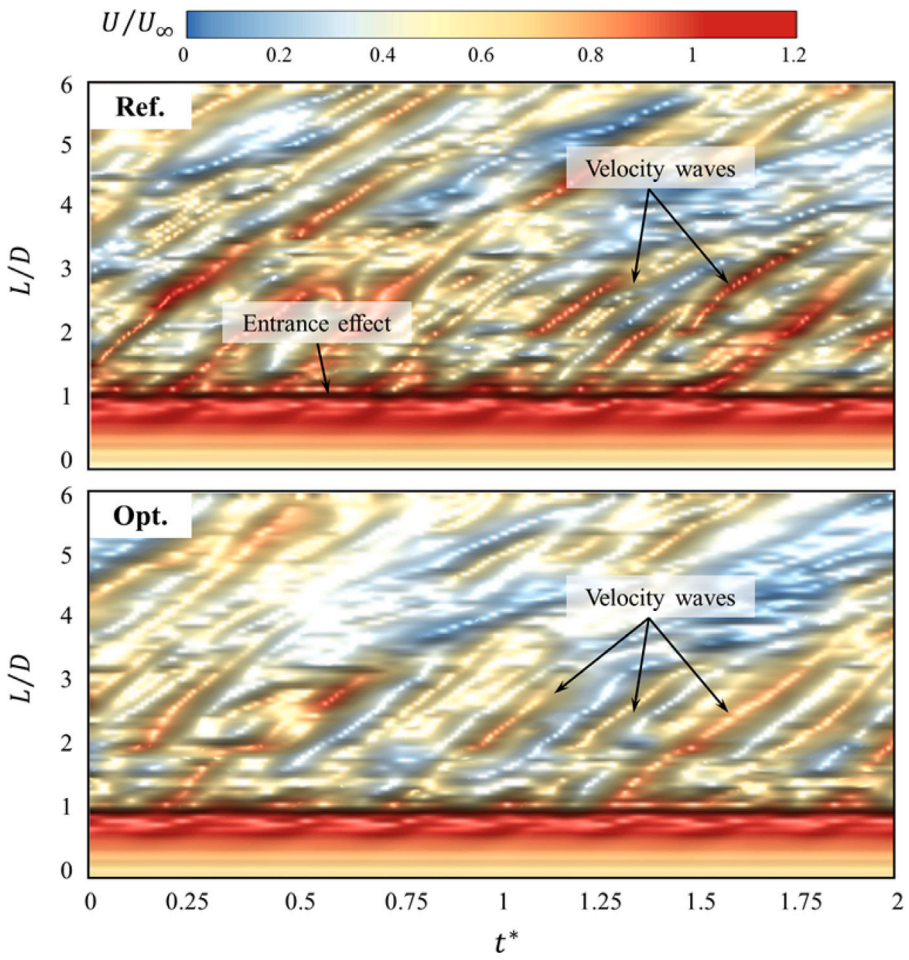

Fig. 22. Time/space distributions of instantaneous normalized velocity magnitude for the reference and optimized cooling holes along the centerline within the hole.

the normalized velocity magnitude distributions in both temporal and spatial domain, computed by the LES approach for the reference and optimized cooling hole configurations. The velocity data is extracted along the centerline of the cooling hole, extending from the inlet to the exit. The horizontal axis represents the time ($t^* = L/U_j$), indicating the time-passing period of the coolant flow through the hole, while vertical axis corresponds to the hole length (L) normalized by the hole diameter (D). As shown in Fig. 22, the velocity magnitude increases gradually from the hole inlet ($L/D = 0$), reaching a peak near $L/D = 1$, indicated by the red color region in the figure. This peak is attributed to the cooling hole entrance effects, which are also evident in Fig. 20(a). Beyond $L/D = 1$, the velocity magnitude decreases due to the onset of a separation region generated near the leeward side of the metering section of the hole. For $L/D > 1$, periodic velocity fluctuations, often referred as velocity waves, are observed. These disturbances are periodically generated and are propagated downstream toward the hole exit over time. It is interesting to note that the slope of these waves reflects the convective velocity of coolant jet along the centerline. In the optimized configuration, the velocity magnitude along the centerline is generally lower than that of the baseline case, especially near the hole exit. This reduction indicates a lower momentum of the coolant jet before it interacts with the mainstream flow, thereby enhancing cooling effectiveness. Furthermore, as shown in Fig. 22, the optimized configuration generates fewer and smoother velocity waves compared to the reference case. This improvement contributes to a more stable internal flow structure and a less wavy velocity pattern, indicating a decrease in turbulence intensity within the cooling hole.

To investigate the influence of cooling hole geometry modifications on flow unsteadiness within the mixing region, the power spectral density (PSD) of the pressure fluctuations computed by the LES approach is analyzed for both the reference and optimized cooling holes, as shown in Fig. 23. The monitoring point is located at the hole exit,

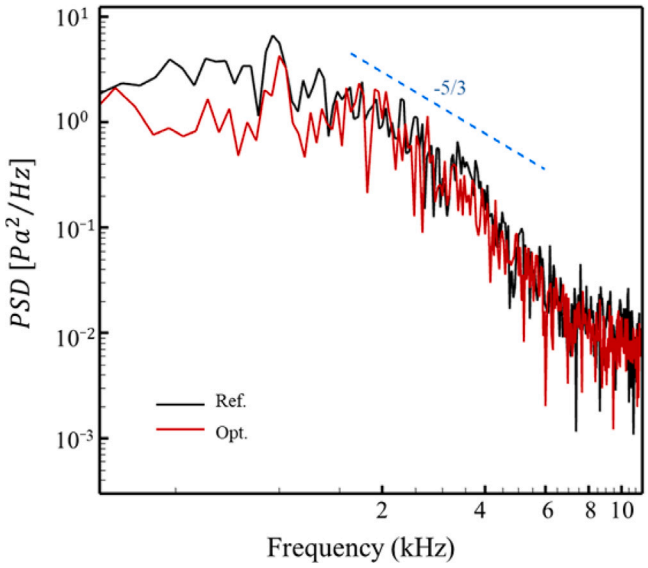

Fig. 23. Power spectral density profiles of pressure fluctuations for the reference and optimized cooling holes, measured at a monitoring point located at $x/D = -2$ and $y/D = 0.1$.

specifically at $x/D = -2$ and $y/D = 0.1$. The PSD offers a frequency-domain representation of the pressure energy distribution, providing valuable insights into unsteady flow characteristics, which are essential for understanding cooling effectiveness. As shown in Fig. 23, although the overall spectrum trends for the optimized geometry resemble those of the reference case, a noticeable reduction in the magnitude of the spectrum baseline, particularly at low frequencies, is observed. This indicates a suppression of coolant jet fluctuations at the hole exit, which suggests a more stable jet structure, reduced mixing, and potentially enhanced cooling performance.

5. Conclusions

In this study, an optimization framework was developed using an LES approach alongside a subdivision surface model shape parameterization and a genetic algorithm-based optimizer. This study focuses on two key geometric variables, mode number and mode amplitude, which were applied to a laidback fan-shaped cooling hole to improve the cooling effectiveness. The LES-WALE method was conducted to obtain the cooling performance for eight modified hole configurations, generated by an LHS DOE approach. The objective was to maximize the area-averaged cooling effectiveness on the flat plate surface downstream of the cooling hole exit. The numerical LES results for the baseline configuration were validated against experimental data to ensure the reliability of the LES predictions.

1. It was shown that surface modifications in the diffuser section of the cooling hole, achieved through modal shape parameterization technique, significantly enhanced film-cooling effectiveness across all designed cases compared to the reference geometry. Among the modified configurations, Case5 exhibited the lowest improvement, with an cooling performance increase of approximately 4% relative to the baseline, and Case6 achieved the highest enhancement, showing an improvement of about 17%.

2. In general, the cases with outward expansion of the hole's cross-sectional area on both the leeward and windward sides showed superior cooling performance. This led to a reduction in the jet TKE near the hole exit and a weakening of the interaction between the jet and mainstream, thereby enhancing surface coverage and cooling performance. Additionally, it improved the lateral distribution of cooling effectiveness by altering the internal separation bubble characteristics and promoting better coolant jet attachment to the flat plate surface.

3. The flow field analysis demonstrated that, in all designed cases, the coolant jet momentum at the hole exit was consistently lower than that of the reference case, contributed to a more favorable jet trajectory within the hole. In the reference geometry, periodic vortical structures were observed at the hole inlet, propagating toward the windward side and extending downstream toward the hole exit. In contrast, the modified cases introduced significant alterations to the internal flow behavior due to change in the diffuser surface. These modifications disrupted the formation of coherent vortical structures and promoted interaction with additional vortices within the diffuser region, preventing their propagation to the hole exit.

4. It was shown that the optimized hole configuration showed improved lateral cooling effectiveness across the entire streamwise distance (x/D) compared to the reference case. The overall film-cooling effectiveness increased by approximately 22%, attributed to the formation of a trench-like feature near the trailing edge of the hole. This geometric characteristic enlarged the internal separation bubble and redirected the coolant jet more effectively toward the windward side, thereby enhancing surface coverage and cooling performance.

5. The time/space evaluation of the instantaneous velocity field within the cooling hole revealed a lower velocity magnitude in the optimized configuration, especially near the hole exit, compared to the baseline case. Additionally, the optimized hole exhibited reduced flow unsteadiness and weaker velocity disturbances relative to the reference hole. These characteristics contributed to a decrease in turbulence intensity and suppressed mixing between the coolant and the mainstream flow at the hole exit.

The presented numerical optimization framework, which integrates LES with a modal shape parameterization technique, has been employed to identify the optimal cooling hole configuration for maximizing cooling performance under fixed blowing and density ratios. In this study, the modal shape parameterization was restricted to modification in the diffuser section of the cooling hole. Future research will extend this approach to encompass a wider range of hole geometries and operating conditions, aiming to provide a more comprehensive understanding of their impact on film-cooling effectiveness.

CRediT authorship contribution statement

Ali Zamiri: Writing – review & editing, Writing – original draft, Visualization, Validation, Supervision, Software, Methodology, Investigation, Formal analysis, Conceptualization. **Sam Lovett:** Writing – original draft, Methodology. **Daniel J. Poole:** Methodology. **Thomas C.S. Rendall:** Writing – original draft, Methodology. **C.B. Allen:** Methodology. **Giovanna Barigozzi:** Writing – review & editing. **Jin Taek Chung:** Writing – review & editing.

Declaration of competing interest

The authors declare that they have no known competing financial interests or personal relationships that could have appeared to influence the work reported in this paper.

Acknowledgment

This work was carried out using the computational facilities of the Advanced Computing Research Centre, University of Bristol - http://www.bristol.ac.uk/acrc/.

Data availability

No data was used for the research described in the article.

References

[1] J.C. Han, S. Dutaa, S. Ekkad, Gas Turbine Heat Transfer and Cooling Technology, CRC Press, 2012.
[2] R.J. Goldstein, Film cooling, Adv. Heat Transf. (7) (1971) 321–379.
[3] J.C. Han, S. Dutta, S. Ekkad, Gas turbine heat transfer: Ten remaining hot gas path challenges, J. Turbomach. (129) (2007) 193–201.
[4] S. Ito, R.J. Goldstein, E.R.G. Eckert, Film cooling of a gas turbine blade, J. Eng. Gas Turbines Power (100) (1978) 476–481.
[5] R. Krewinkel, A review of gas turbine effusion cooling studies, Int. J. Heat Mass Transfer (66) (2013) 706–722.
[6] J. Town, D. Straub, J. Black, K.A. Thole, T.I.P. Shih, State-of-the-art cooling technology for a turbine rotor blade, J. Turbomach. (140) (2018) 071007.
[7] R.J. Goldstein, E.R.G. Eckert, F. Burggraf, Effects of hole geometry and density on three-dimensional film cooling, Int. J. Heat Mass Transfer (17) (1974) 595–607.
[8] H. Abdeh, G. Barigozzi, A. Zamiri, J.T. Chung, Pressure sensitive paint and large eddy simulation investigation on the impact of trench depth on flat plate film cooling through shaped holes, J. Turbomach. (146) (2024) 051001.
[9] A. Zamiri, S.J. You, J.T. Chung, Large eddy simulation of unsteady turbulent flow structures and film-cooling effectiveness in a laidback fan-shaped hole, Aerosp. Sci. Technol. J. (66) (2020) 706–722.
[10] A.K. Sinha, D.G. Bogard, M.E. Crawford, Film-cooling effectiveness downstream of a single row of holes with variable density ratio, J. Turbomach. (113) (1991) 442–449.
[11] R.P. Schroeder, K.A. Thole, Adiabatic effectiveness measurements for a baseline shaped film cooling hole, ASME Pap. (2014).
[12] A. Zamiri, G. Barigozzi, J.T. Chung, Large eddy simulation of film cooling flow from shaped holes with different geometrical parameters, Int. J. Heat Mass Transfer (196) (2022) 123261.
[13] J.J. Hu, B.T. An, Film cooling effectiveness investigation of diffusion slot holes on a turbine guide vane leading edge, Int. Commun. Heat Mass Transfer (158) (2024) 107845.

[14] K. Kusterer, D. Bohn, T. Sugimoto, R. Tanaka, Double-jet ejection of cooling air for improved film cooling, J. Turbomach. (129) (2007) 809–815.
[15] K. Kusterer, A. Elyas, D. Bohn, T. Sugimoto, R. Tanaka, M. Kazari, The NEKOMIMI cooling technology: Cooling holes with ears for high-efficient film cooling, ASME Pap. (2011).
[16] E. Sakai, T. Takahashi, Numerical study on effects of density ratio on film cooling structure and flim cooling effectiveness, ASME Pap. (2017) GT2017–63168.
[17] Y. Lu, A. Dhungel, S.V. Ekkad, R.S. Bunker, Effect of trench width and depth on film cooling from cylindrical holes embedded in trenches, J. Turbomach. (131) (2009) 13.
[18] R.S. Bunker, A review of shaped hole turbine film cooling technology, J. Heat Transf. (127) (2005) 441–453.
[19] A. Zamiri, G. Barigozzi, J.T. Chung, Large eddy simulation of film cooling flow from shaped holes with different geometrical parameters, Int. J. Heat Mass Transfer (196) (2022) 123261.
[20] S.H. Park, Y.J. Kang, H.J. Seo, J.S. Kwak, Y.S. Kang, Experimental optimization of a fan-shaped film cooling hole with 30 degrees-injection angle and 6-hole length-to-diameter ratio, Int. J. Heat Mass Transfer (144) (2019) 118652.
[21] Y.R. Jo, J.Y. Jeong, J.S. Kwak, Experimental optimization of the compound angled asymmetric laidback fan shaped film cooling hole, Energies J. (15) (2022) 7985.
[22] J.Y. Jeong, Y.R. Jo, G.M. Kim, Y.J. Kang, M.S. Kang, J.S. Kwak, Experimental optimization of butterfly-shaped film cooling hole configuration with a 30 degree injection angle, Int. J. Heat Mass Transfer (227) (2024) 125568.
[23] Y. Jiang, Z. Tao, H. Li, Z. Zhou, Shape optimization of the laidback fan-shaped film cooling hole on pressure surface of turbine guide vane, ASME Pap. (2022) GT2022–82358.
[24] H. Zhang, Y. Li, Z. Chen, X. Su, X. Yuan, Multi-fidelity model based optimization of shaped film cooling hole and experimental validation, Int. J. Heat Mass Transfer (132) (2019) 118–129.
[25] F.B. Jones, D.W. Fox, T. Oliver, D.G. Bogard, Parametric optimization of film cooling hole geometry, ASME Pap. (2021).
[26] A. Zamiri, S.J. You, J.T. Chung, Surface roughness effects on film-cooling effectiveness in a fan-shaped cooling hole, Aerosp. Sci. Technol. J. (119) (2021) 107082.
[27] S. Agarwal, L. Gicquel, F. Duchaine, N. Odier, J. Dombard, D. Bonneau, M. Slusarz, Large eddy simulation based optimization of a fan-shaped cooling hole geometry to enhance cooling performance, ASME Pap. (2022) GT2022–79923.
[28] A. Zamiri, J.T. Chung, Large eddy simulation of compound angle effects on cooling effectiveness and flow structure of fan-shaped holes, Int. J. Heat Mass Transfer (178) (2021) 121599.
[29] A. Zamiri, G. Barigozzi, J.T. Chung, Large eddy simulation of in-hole blockage effects on cooling performance of fan-shaped holes, Int. Commun. Heat Mass Transfer (159) (2024) 108100.
[30] A. Zamiri, J.T. Chung, Large eddy simulation of internal coolant crossflow orientation effects on film-cooling effectiveness of fan-shaped holes, Int. J. Heat Mass Transfer (190) (2022) 122778.
[31] A. Zamiri, S.J. You, J.T. Chung, Large eddy simulation in the optimization of laidback fan-shaped hole geometry to enhance film-cooling performance, Int. J. Heat Mass Transfer (158) (2020) 120014.
[32] Star-CCM+ Theory Guide, Simcenter STAR-ccm+ documentation, 2023.
[33] S.V. Patankar, Numerical Heat Transfer and Fluid Flow, McGraw-Hill, Washington, New York, London, 1980.
[34] M.S. Darwish, F. Moukalled, Normalized variable and space formulation methodology for high-resolution schemes, Numer. Heat Transf. J. PArt B (26) (1994) 79–107.
[35] D. Masters, N.J. Taylor, T. Rendall, C. Allen, D. Poole, Geometric comparison of aerofoil shape parameterization methods, AIAA J. 55 (5) (2017).
[36] E. Catmull, J. Clark, Recursively generated B-spline surfaces on arbitrary topological meshes, Computer-Aided Des. 10 (6) (1978).
[37] S. Lovett, T. Rendall, J. De Courcy, C. Allen, D. Poole, N.J. Taylor, J. Fincham, M. Wood, N. Leppard, Modal analysis of subdivision surfaces for aerodynamic shape parameterisation, in: AIAA Aviation Forum and Ascend, 2025.
[38] D. Masters, N.J. Taylor, T. Rendall, C. Allen, Multilevel subdivision parameterization scheme for aerodynamic shape optimization, AIAA J. 55 (10) (2017).
[39] C. Loop, Smooth Subdivision Surfaces Based on Triangles (Ph.D. thesis), The University of Utah, 1987.
[40] M.A. Halstead, M. Kass, T. DeRose, Efficient, fair interpolation using catmull–clark surfaces, in: Proceedings of the 20th Annual Conference on Computer Graphics and Interactive Techniques, 1993.
[41] M.D. McKay, R.J. Beckman, W.J. Conover, A comparison of three methods for selecting values of input variables in the analysis of output from a computer code, Technometrics J. 21 (2) (1979) 239–245.
[42] F.A.C. Viana, R.T. Haftka, V.S. Jr., Multiple surrogates: How cross-validation errors can help us to obtain the best predictor, Struct. Multidiscip. Optim. J. 39 (2) (2009) 439–457.
[43] A. Zamiri, J.T. Chung, Large eddy simulation of internal coolant crossflow orientation effects on film-cooling effectiveness of fan-shaped holes, Int. J. Heat Mass Transfer (190) (2022) 122778.